Thesis Dissertation

THERMAL IMAGE QUALITY ASSESSMENT AND VALIDATION FOR BREAST CANCER CLASSIFIER INFERENCE

Andreas Tamanis

UNIVERSITY OF CYPRUS

COMPUTER SCIENCE DEPARTMENT

December 2025

UNIVERSITY OF CYPRUS

COMPUTER SCIENCE DEPARTMENT

Thermal Image Quality Assessment and Validation for Breast Cancer Classifier Inference

Andreas Tamanis

Supervisor

Dr. Christodoulou Christos

A thesis submitted in partial fulfillment of the requirements for the award of Bachelor's degree in Computer Science at the University of Cyprus

December 2025

Acknowledgements

I would like to express my sincere gratitude to my supervisor, Professor Christodoulou Christos, for their guidance, trust, and feedback throughout the course of this thesis. Their insights and encouragement were of great value for this work and helped me navigate both the technical and academic aspects of the research process.

I would also like to than Mr. Pafitis Marios, co-founder of MammoCheck, for his guidance and practical insights throughout this work. His input on real-world constraints and requirements for thermal imaging breast cancer screening helped inform the direction of this thesis and ensured that the proposed pipeline addressed meaningful and relevant challenges.

Finally, I would like to thank my family for their constant support, patience, and encouragement throughout my studies. Their belief in me and their continued support made it possible for me to complete this work.

Abstract

Thermal imaging has emerged as a promising, non-invasive technique for breast cancer screening, particularly when combined with artificial intelligence-based analysis. However, the reliability of such systems strongly depends on the quality and consistency of the acquired thermal images. Variations in image sharpness, background thermal activity, patient pose, and chest preparation can significantly degrade the performance of downstream classification models.

This thesis presents a rule-based quality assessment pipeline designed to evaluate thermal breast images prior to automated breast cancer classification. The proposed pipeline operates sequentially and includes checks for image sharpness, background cleanliness, binary pose validity, anatomical landmark geometry, and breast band thermal quality. A combination of image processing techniques and lightweight deep learning models is used to detect and reject images that violate acquisition and quality constraints.

The pipeline was evaluated using the DMR-IR thermal imaging dataset through qualitative analysis and representative examples. The results demonstrate that each individual check behaves as intended, effectively identifying common acquisition errors such as blur, incorrect positioning, background thermal artefacts, occlusions, and insufficient cooling. By filtering unsuitable images early in the process, the pipeline helps standardize input conditions and reduces the likelihood of unreliable downstream analysis.

Rather than serving as a diagnostic system, this work establishes a foundation for automated quality assessment in thermal breast cancer screening. The proposed pipeline provides a structured and extensible framework that supports the development of more robust and reliable artificial intelligence-based screening systems, including those envisioned by MammoCheck.

Contents

1 Introduction

1.1 Background

Thermal imaging is a technique used across many scientific fields. Thermal cameras measure the infrared radiation emitted by surfaces and map these measurements to form a temperature-based image. As a result, each pixel corresponds to a temperature intensity value. The amount of emitted infrared radiation is directly linked to the surface temperature of biological tissue. Because temperature variations reflect physiological processes such as blood flow or inflammation, thermal imaging has also been adopted in medical analysis. Due to its non-invasive, contact-free, radiation-free, and cost-effective nature, many researchers have explored thermal imaging as a way to enhance, or even replace, certain conventional imaging techniques in the medical sector [1].

The breast area can exhibit thermal activity that carries valuable information for detecting abnormalities in the tissue. These abnormalities may be associated with variations in blood flow, inflammation, or elevated metabolic activity, all of which create localized temperature changes. Through thermal image analysis, such changes can complement conventional screening techniques by providing insight into an area's heat distribution rather than relying solely on structural information. These thermal patterns, however, are often subtle and difficult to interpret visually, which is why machine learning models play a significant role in processing them. Neural networks excel at extracting patterns and features in cases where the naked eye may struggle. For these models to perform reliably, the input data is expected to have a degree of consistency, proper framing, and an absence of distortions. Variations affecting thermal image quality therefore create significant challenges for automated classification systems.

Furthermore, variations in thermal image quality can differ greatly between images gathered in controlled research environments, actual screening sessions conducted by briefly trained personnel, or even home self-tests. There are many external factors that can affect the quality of a thermal capture. Slight patient movement or incorrect camera settings can lead to image blur, while incorrect body posture or the presence of artefacts can obscure important anatomical regions. In addition, noisy environmental conditions or inconsistent body cooling can weaken or distort the thermal signatures needed to reveal critical details [2].

MammoCheck [3] is a Cyprus-based MedTech startup developing a Software as Medical Device (SaMD) platform designed to assist in the early detection of breast cancer using AI-powered thermal imaging analysis. Their approach integrates proprietary deep learning algorithms trained on thermal breast images to detect temperature anomalies that may indicate abnormal cellular activity or blood flow patterns associated with cancer development.

MammoCheck positions its technology as a complementary screening tool to traditional mammography, particularly targeting underserved populations including women under 45 (for whom mammography is not routinely recommended), women with dense breast tissue (where mammography has limitations), and those in healthcare deserts with limited access to screening facilities. The platform combines affordable consumer-grade thermal cameras (off-the-shelf devices with smartphone connectivity) with cloud-based AI processing infrastructure that analyzes thermal images typically within seconds. This approach enables radiation-free, pain-free, at-home breast examinations through mobile applications available on both iOS and Android platforms.

The importance of obtaining consistent, high-quality thermal images in uncontrolled home environments, as opposed to clinical laboratory settings, presents a significant technical challenge that directly motivates the need for an automated quality-assessment pipeline such as the one proposed in this thesis.

1.2 Problem Statement

AI-based breast cancer classifiers rely heavily on receiving clear and properly captured thermal images [4]. When the input image is blurred, poorly posed, occluded, or cropped in a way that hides important anatomical regions, the classifier's predictions become unreliable. In real screening scenarios, especially those outside controlled laboratory environments, it is common to encounter thermal images that do not meet the minimum quality requirements. This issue is present in the MammoCheck [3] workflow as well, since images are collected by operators with different levels of experience and under varying conditions. The classifier used by MammoCheck cannot be expected to produce stable or meaningful results when the input image is misaligned, incomplete, or contaminated with artefacts. Relying on manual inspection to filter out these problematic images is slow, subjective, and impractical as the number of screenings grows. At the moment, there is no automated mechanism in place to detect and remove invalid thermal breast images before they are passed to a classifier. This

creates the need for a reliable and systematic quality-assessment process that can evaluate each image and decide whether it is suitable for further analysis.

1.3 Motivation

The reliability of any machine learning system depends not only on how the model is trained but also on the quality of the data it receives during inference. For thermal breast cancer screening, this becomes even more important, since the model is expected to interpret subtle temperature variations that can easily be distorted by poor image capture. Ensuring that only well-framed, sharp, and unobstructed images reach the classifier is therefore essential for obtaining trustworthy results.

This need becomes clear, since MammoCheck aims to allow patients to capture thermal images of themselves at home, where inconsistencies and distortions have a higher possibility of appearing. Furthermore, if an error does appear in the thermal capture, a proper reasoning should be formed to allow the patients being screened to adjust accordingly and eliminate errors that would lead to unreliable diagnosis.

Without an automated way of filtering out invalid images, the system remains vulnerable to unpredictable errors and inconsistent predictions. Creating a dedicated quality-assessment pipeline is therefore an important step toward making thermal-based screening more reliable, scalable, and suitable for real-world use.

1.4 Objectives

The main objective of this thesis is to design and implement an automated explainable quality-assessment pipeline capable of identifying whether a thermal breast image is suitable for classification, or explain the reasons of failure when it is not. To achieve this, the work focuses on several specific goals:

- Develop a sharpness evaluation method based on the Laplacian filter to detect blurred or unfocused images.
- Validate body pose using binary masks and silhouette features to ensure that the patient's stance matches the expected capture conditions.
- Assess the background region for noise, artefacts, and inconsistencies that may interfere with the thermal signature of the breast area.

- Detect anatomical landmarks using a CNN model and analyze their geometry to confirm proper breast positioning and symmetry.
- Evaluate breast band quality by examining coverage, symmetry, and intensity patterns that may indicate incomplete body preparation, occlusions or invalid captures.
- Integrate all checks into a unified decision process that labels each thermal image as valid or invalid before it is passed to the MammoCheck classifier.

These objectives collectively aim to ensure that only reliable and properly captured thermal images are used during inference, improving both the stability and the trustworthiness of the downstream classification system.

1.5 Thesis Contributions

This thesis presents several contributions toward improving the reliability of thermal breast image classification systems. The main contributions are summarized as follows:

- A complete multi-stage quality assessment pipeline designed specifically for thermal breast imaging, capable of detecting a wide range of issues such as blur, incorrect pose, insufficient thermal detail, occlusions, and background artefacts.
- A sharpness evaluation method based on the variance of the Laplacian, used to automatically identify unfocused or low-detail thermal images.
- A pose validation component that uses binary masks and silhouette characteristics to detect improper patient positioning and framing.
- A background quality analysis module that evaluates thermal noise, mask consistency, and artefacts that may interfere with classifier reliability.
- An anatomical landmark detection system, built using a YOLO-based model, which verifies breast, nipple, and armpit positioning through geometric relationships.
- A breast band quality check that introduces new metrics such as coverage, symmetry, cutoff detection, intensity imbalance, and occlusion clustering to assess the validity of the breast region.
- A unified decision logic framework that integrates all individual checks into a final valid/invalid classification step suitable for use in the MammoCheck inference pipeline.

Together, these contributions form a robust foundation for automated thermal image validation for AI-based breast cancer screening.

1.6 Thesis Structure

The remainder of this thesis is organized into the following chapters:

- **Chapter 2 - Literature Review:**
  Presents the theoretical background and related work on thermal imaging, image quality assessment, pose estimation, background segmentation, and breast band thermal quality. It also discusses existing approaches in breast thermography and highlights the research gaps that motivated this work.
- **Chapter 3 - Dataset and Preprocessing:**
  Describes the dataset used in this work and the preprocessing steps applied to the thermal images. It includes an overview of the DMR-IR database, image acquisition protocols, and the generation of datasets required for pose validation and anatomical landmark detection.
- **Chapter 4 - Methodology:**
  Presents the proposed methodology and technical implementation of the quality assessment pipeline. The chapter explains each processing stage in detail, including sharpness evaluation, background quality analysis, pose validation, anatomical landmark checks, and breast band quality assessment for different viewing angles.
- **Chapter 5 - Results and Evaluation:**
  Presents the experimental results and evaluation of the proposed pipeline. This includes the training performance of the YOLO-based models, as well as qualitative and quantitative results demonstrating the behavior and effectiveness of each quality check.
- **Chapter 6 - Discussion:**
  Discusses the experimental setup and interprets the results obtained. The strengths and limitations of the proposed approach are examined, and its behavior under the evaluated conditions is analyzed.
- **Chapter 7 - Conclusion and Future Work:**
  Concludes the thesis by summarizing the main findings and contributions of the work.

It also outlines directions for future research and potential extensions of the proposed quality assessment pipeline.

2 Literature Review

2.1 Thermal Imaging in Medical Applications

The use of thermal imaging for medical assessment has been explored for several decades, and it remains relevant across many clinical applications. Under appropriate acquisition conditions, thermal screenings can assist in detecting inflammation, arthritis, vascular abnormalities, diabetic foot complications, fever, and other physiological issues by analyzing texture patterns, intensity distributions, or thermal asymmetries in the affected regions [5] [6] [7]. Interest in expanding these applications continues, largely because thermal imaging is non-invasive, contact-free, safe for repeated use, and relatively inexpensive compared to many traditional modalities.

However, medical thermal screening also presents challenges. Reliable measurements require minimal environmental noise, controlled temperature conditions, and proper patient positioning, making the process sensitive to operator technique. In recent years, thermal imaging has gained significant attention for breast cancer detection, particularly through the use of machine learning models that rely on advanced architectures and data-processing methodologies [8]. Given the clinical importance of the task, it is essential that the thermal data used during inference is of high and consistent quality. This is typically supported by capture protocols and patient preparation guidelines designed to minimize variability. These protocols typically require the patient to be fully undressed from the waist up, to adopt specific standardized poses that avoid obstructing the chest or breast area, and to maintain a consistent body orientation relative to the camera. Patients are also given time to undergo thermal acclimatization, allowing their body temperature to stabilize in a uniform manner so that physiological details, such as vascular activity in the chest, are more accurately represented.

2.2 Medical Image Quality Assessment

The quality of an image used in medical settings plays a critical role in diagnostic performance, since distortions, blur, or occlusions can easily lead to incorrect interpretations. AI-based systems are particularly sensitive to variability in input quality, and consistent, high-quality images are essential for producing stable and reliable inference results [4].

Medical images can suffer from a wide range of degradation types, depending on the acquisition conditions, equipment, and operator technique. These include motion blur, out-of-focus blur, noise, occlusions, incorrect patient pose, or the exclusion of important anatomical regions from the frame. Such problems can disrupt diagnostic workflows, reduce the accuracy of automated analysis, and undermine downstream decision-making. Research in Medical Image Quality Assessment aims to characterize these issues and develop methods for evaluating and improving image quality, often through metrics that quantify sharpness, noise levels, contrast, anatomical coverage, and the presence of artefacts [9].

2.3 Pose Estimation in Computer Vision

Pose estimation is a major part in computer vision that aims to determine the spatial shape of a body by detecting key anatomical landmarks. With the use of deep learning, modern approaches have significantly improved the accuracy of such detections, enabling reliable estimation of variations in pose [10] [11]. Landmark-based representations are widely used in action recognition and gesture analysis, as they provide geometric information that can be used to determine human posture [12].

Binary silhouettes have also been used in several computer vision studies as a lightweight representation for human pose classification. Even without texture or color information, silhouettes capture essential geometric properties of the body, such as limb orientation, torso symmetry, and overall stance, which can be sufficient for distinguishing between different postures [13]. Prior work has shown that pose characteristics can be reliably inferred from silhouettes alone, and that such representations remain effective under variations in lighting or appearance. In this thesis, a similar idea is applied in a simpler form. Binary body masks are used to model examples of correct and manually generated incorrect poses, allowing a YOLO classifier to learn the distinction between valid thermal screening poses with arms in expected positions, and invalid ones with arms not raised properly. This approach was

necessary because the dataset did not contain enough real images of invalid poses, particularly cases where the patient's arms were lowered or covering the chest.

Recent work has adopted object detection frameworks to improve landmark localization. Detection based models such as the YOLO family have proven effective for fast and accurate localization of keypoints in complex scenes [14]. Variations of YOLO have been adapted for pose estimation by predicting anatomical landmarks instead of generic object classes. For example, Dong and Du demonstrated that a modified YOLOv8 architecture can achieve high performance in human pose estimation tasks, even under challenging acquisition conditions [15].

In thermal breast imaging, landmark detection serves a more specialized purpose. Instead of capturing the full body configuration, the goal is to localize specific anatomical parts such as the breasts, nipples, and armpits, that indicate patient orientation, symmetry, and pose validity. Similar ideas have been applied in medical imaging, where landmark detection is used to guide alignment, segmentation, and diagnostic measurements [16]. In thermal images, where texture information is limited and anatomical details can be subtle, detection-based approaches offer a practical and reliable way to parse body geometry. These considerations motivate the use of a YOLOv8 landmark detector in the quality assessment pipeline developed in this thesis.

2.4 Background Segmentation and Evaluation

Thermal breast images often contain large portions of background, including walls, equipment, reflections, or objects present in the screening environment. These elements introduce temperature noise that can interfere with the interpretation of thermal patterns on the body, especially when the background contains strong gradients or artefacts. To mitigate these effects, most automated thermography pipelines isolate the breast and torso region before any diagnostic or machine learning analysis is performed [17].

A variety of segmentation approaches have been explored. Early work relied on thresholding, morphological operations, or region-growing methods, while more recent studies have adopted clustering algorithms and convolutional neural networks to obtain cleaner breast masks [18]. Segmentation is typically treated as a preprocessing step that ensures only relevant anatomical regions are passed to subsequent classification models.

However, these methods focus primarily on extracting the breast region rather than evaluating the quality of the segmentation itself. They generally assume that the silhouette is complete and that the background does not introduce distortions. In practice, thermal images may contain broken masks, excessive background coverage, or artefacts that compromise downstream analysis. While some studies acknowledge the impact of background noise on thermographic interpretation [19], there is limited work on using background characteristics as a criterion for determining whether an image is suitable for further processing. This gap motivates the background-quality checks incorporated into the pipeline developed in this thesis.

2.5 Breast Band Quality

Many studies in breast thermography emphasize the importance of obtaining images where the breast region is fully visible and free from external obstructions. Occlusions caused by clothing, hair, or medical bandages can distort the thermal signature or conceal relevant temperature patterns, making the resulting image unsuitable for analysis [20]. Since thermal abnormalities are often subtle, even small obstructions can interfere with downstream interpretation or lead to misclassification.

Existing thermography research typically assumes that the breast area has been captured correctly and that no major occlusions are present. In practice, however, clinical or home screening environments frequently produce images where parts of the breast are cropped, partially covered, or hidden by pose variations. Several studies have noted that improper positioning or coverage of the breast region reduces diagnostic reliability and should ideally be avoided during acquisition [21]. Although some recent work incorporates automated segmentation to isolate the breast region, these methods rarely assess whether the segmented area is complete or affected by artefacts [19].

The lack of dedicated tools for evaluating breast-region visibility and detail motivates the need for explicit occlusion and coverage checks. In this thesis, a “breast band” quality assessment is used to measure the symmetry, continuity, and completeness of the breast region and to detect cases where thermal details are missing or obstructed. This provides an additional safeguard before thermal images are forwarded to the classification model.

2.6 Summary of Research Gaps

Although thermal imaging has been widely explored for medical applications and breast thermography has seen growing interest with the rise of machine learning methods, most existing approaches focus on classification or feature extraction rather than on assessing image validity. Prior work generally assumes that thermal images are correctly captured, properly segmented, well-focused, and free of occlusions or background artefacts. In practice, however, real screening environments frequently produce images with inconsistent pose, blurry regions, incomplete anatomical coverage, and variable background noise. Current segmentation methods attempt to isolate the breast region but do not evaluate whether the resulting mask is accurate or suitable for analysis. Similarly, pose estimation studies rarely address the specific constraints of thermal breast imaging. As a result, there is a clear gap in the literature regarding automated quality assessment for thermal breast images, which this thesis aims to address through a multi-stage pipeline designed to detect invalid or unreliable captures.

3 Dataset and Preprocessing

3.1 Dataset Overview

The DMR-IR database [22] used in this thesis contains thermal images of 141 patients classified as healthy or unhealthy, captured from five different angles: Front (0°), Right Lateral 45°, Right Lateral 90°, Left Lateral 45°, and Left Lateral 90°, as shown in Figure 1. The dataset was created to support research on patient preparation and room conditioning protocols for thermal breast screenings, as well as to complement existing thermal datasets used in breast cancer analysis. All images were acquired using a FLIR SC620 infrared camera with a thermal sensitivity of 0.04°C, a resolution of 640 × 480 pixels, and are in grayscale.

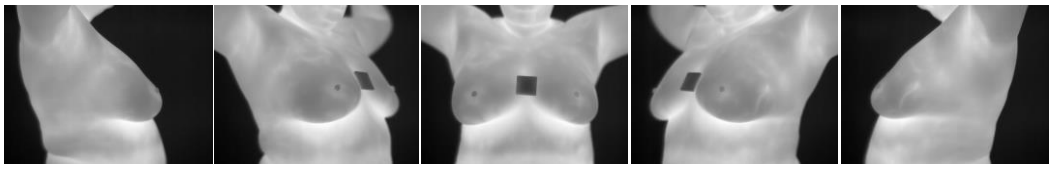

Figure 1: A patient's collection of images

The images are captured in a controlled environment with a room temperature of approximately 21°C (±1°C) and a relative humidity of around 60% (±5%). Prior to imaging, the patient undergoes a cooling period of roughly 20 minutes with minimal physical activity, which helps stabilize temperature and enhances the visibility of thermal patterns in the breast region. In addition, the skin is kept free of lotions, sweat, or alcohol-based substances before and after the cooling period to avoid artefacts caused by surface temperature irregularities [22].

It is important to note that, because the dataset was collected under controlled experimental conditions, very few images exhibit incorrect patient positioning, occlusions, or noticeable artefacts. While this consistency is beneficial for research on cancer detection, it presented a challenge for this thesis, as the quality assessment pipeline developed here requires examples of both valid and invalid captures to evaluate pose correctness, background quality, and occlusion behavior.

3.2 Image Structure

As described in the Dataset Overview, all thermal images have a resolution of 640 × 480 pixels are stored as grayscale intensity maps, so each pixel holds an intensity value between 0 and 255. Each image frames the patient's torso from the neck to the upper abdomen, ensuring that shoulders and armpits are fully visible at the top corners of the frame. During acquisition, patients are instructed to raise their arms above their head and to clamp their hair so that it does not appear within the thermal field of view. They are also required to remove all clothing and accessories, including necklaces and earrings, to prevent unwanted thermal reflections or occlusions.

3.3 Preprocessing Steps

3.3.1 Binary invalid pose dataset generation

For the pose validation stage of the pipeline, the chosen approach was to classify each thermal image using a YOLO-based model trained to distinguish between valid and invalid patient poses. Since the DMR-IR database contains almost exclusively valid images, it was necessary to create a dedicated dataset that included examples of both categories. This required generating additional samples that simulated improper posture, as very few real invalid poses existed in the original dataset.

To generate the invalid pose dataset, binary body images extracted from the valid images were manually edited to create silhouettes representing common incorrect poses. These included samples where the arms were lowered, unevenly raised, or positioned in a way that obscured parts of the chest region, see Figure 3. The resulting binary silhouettes were then converted into image samples compatible with YOLO training, forming a balanced dataset of valid and invalid examples. This dataset enabled the classifier to learn the characteristic geometric patterns associated with incorrect patient positioning.

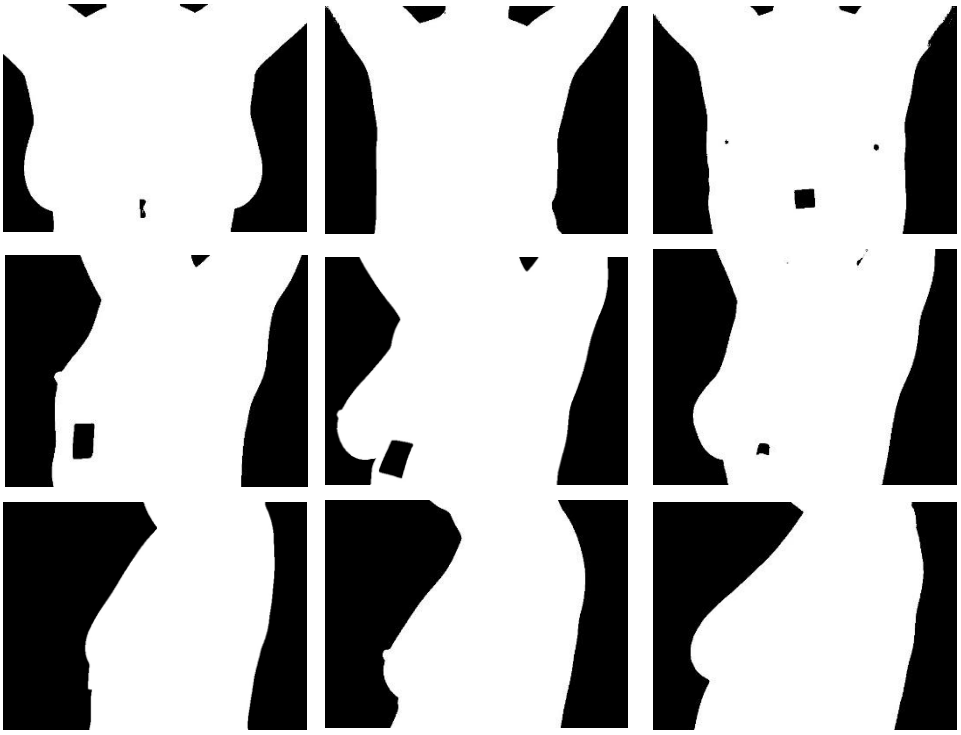

Figure 2: Valid binary silhouettes

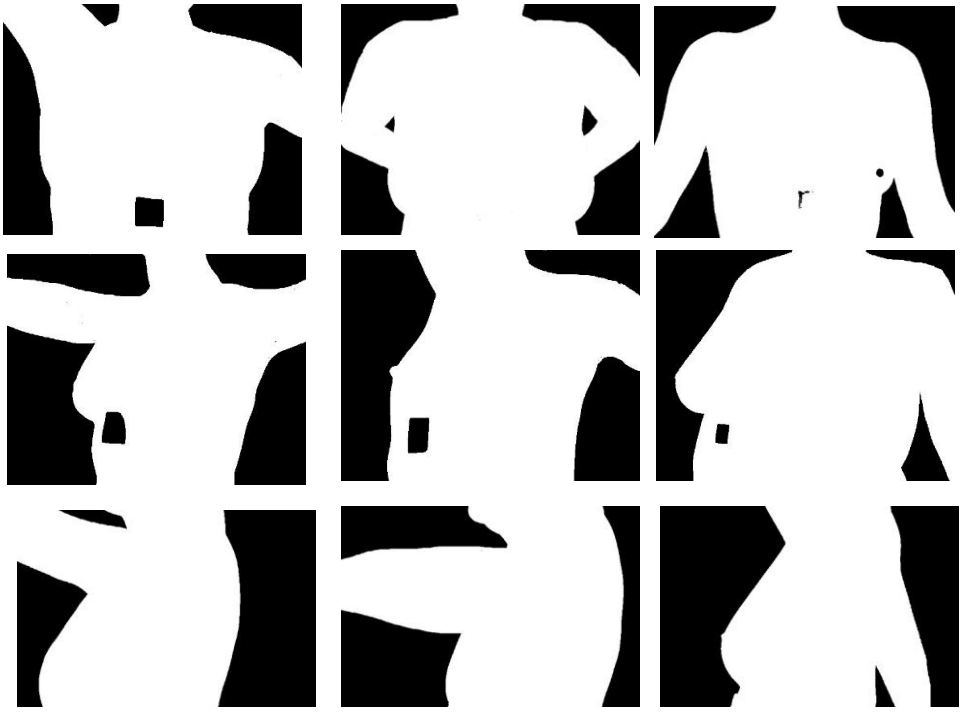

Figure 3: invalid binary generated silhouettes

3.3.2 Anatomical landmark detection dataset labeling

To support pose validation and breast-region analysis in later stages of the pipeline, a YOLO-based landmark detector is used to identify key anatomical points in each thermal image. The model predicts bounding boxes for structures such as breasts, nipples, and armpits, providing additional geometric information that cannot be obtained from the silhouette alone. These landmarks serve as references for evaluating symmetry, orientation, and proper visibility of the breast area during image acquisition.

During preprocessing, bounding boxes were manually placed on each thermal image to mark the anatomical landmarks of interest. The placement was done carefully to ensure that the box edges aligned closely with the true boundaries of each landmark, avoiding unnecessary gaps or excessive padding. This level of precision was important because the later geometric calculations rely not only on the presence of the landmarks, but also on their exact size, shape, and location within the frame.

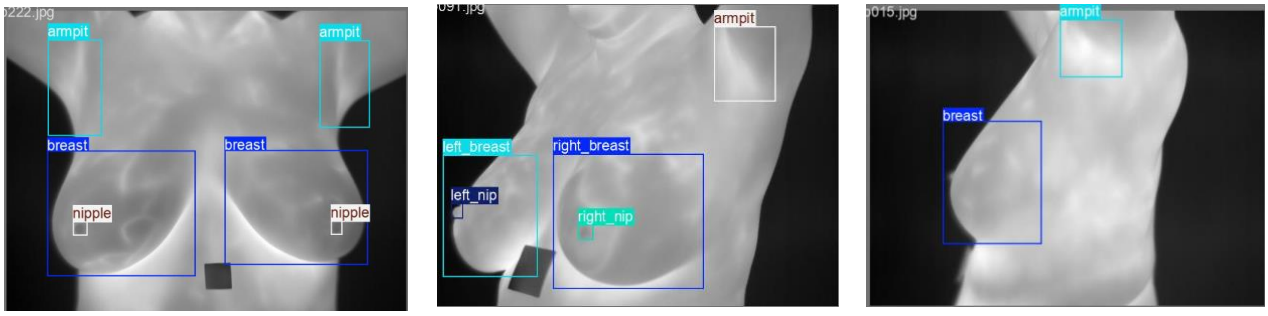

Figure 4: Examples of labeled images

4 Methodology

4.1 Technical Background

4.1.1 Grayscale images

Grayscale images are single-channel images in which each pixel represents an intensity value rather than a color. Instead of storing separate red, green, and blue components, a grayscale image contains only one value per pixel, typically ranging from dark (low intensity) to bright (high intensity). Thermal cameras can be represented in grayscale because they record infrared radiation and convert it into intensity values that correspond to temperature variations. This simplifies processing, since all computations are performed on a single channel rather than on multiple color channels.

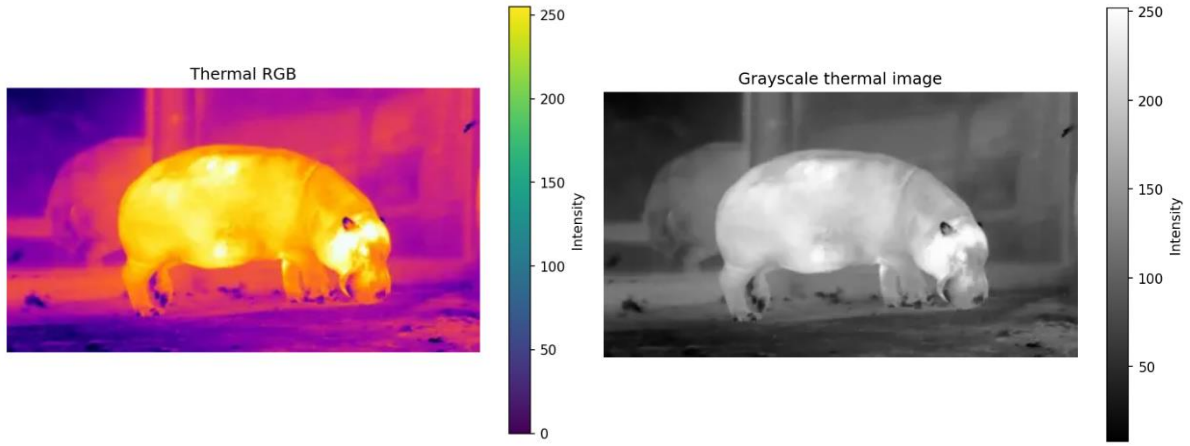

Figure 5: Thermal RGB and Thermal Grayscale Image

4.1.2 The Laplacian filter

The Laplacian filter is an edge-detection operator that highlights areas in an image where the intensity changes rapidly. It works by computing the second derivative of the image, which produces strong responses along edges and fine details. Flat or smooth regions produce low values, while sharp transitions produce high values. Because of this behaviour, the Laplacian is commonly used to assess image sharpness and detect blur. In thermal imaging, it provides a quick way to evaluate whether an image contains enough edge detail to be considered in focus.

Figure 6: The Laplacian filter

4.1.3 Binary conversion

4.1.3.1 Otsu threshold

Binary conversion is the process of turning a grayscale image into a two-level image where each pixel is classified as either 0 (black) or 1 (white) based on their intensities. To perform this automatically, Otsu's thresholding is used. Otsu's algorithm analyzes the image histogram and selects the threshold value that best separates the pixel intensities into two groups. This removes the need for manual tuning and works well when the object of interest has noticeably different intensity values from the background. For thermal images, where the body is typically warmer than the surrounding environment, Otsu's method provides a simple and effective way to generate the initial body mask.

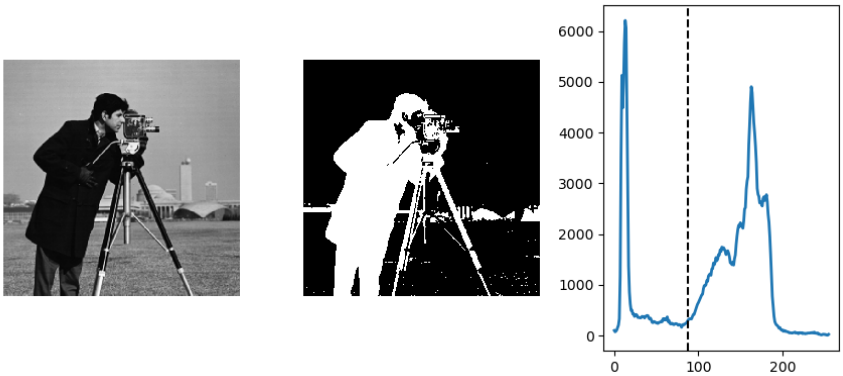

Figure 7: Otsu's threshold

4.1.3.2 Binary Masks

A binary mask is a binary image that is used to conduct operations on specific pixels of an image. This allows many image-processing tasks, such as segmentation, object isolation, or region-based analysis to focus only on selected areas without altering the rest of the image.

Binary masks are therefore a simple but versatile tool for controlling which parts of an image are included in a given operation.

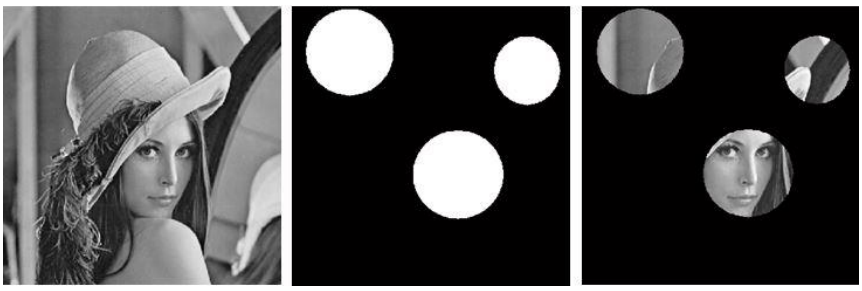

Figure 8: A binary mask used to isolate regions of an image

4.1.3.3 Erosion

Erosion is a fundamental morphological operation used in binary image processing to shrink foreground regions. The operation works by removing pixels from the boundaries of foreground objects based on a predefined structuring element. As a result, thin connections, small protrusions, and isolated noise pixels are eliminated, while larger structures are preserved. Erosion is commonly used to remove small artefacts and to create separation between objects or between an object and its boundary.

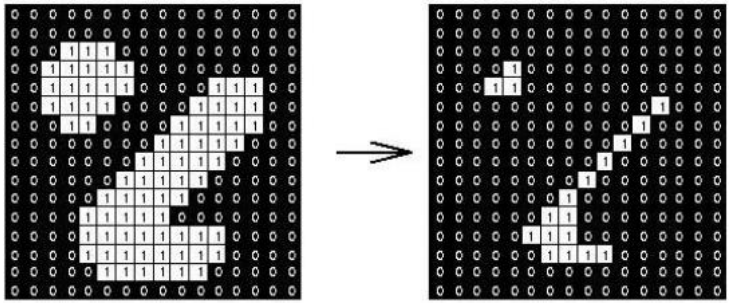

Figure 9: Example of erosion applied on a binary mask

4.1.3.4 Dilation

Dilation is a morphological operation that expands foreground regions in a binary image. Using a structuring element, dilation adds pixels to object boundaries, filling small gaps and closing narrow breaks within foreground regions. This operation is often applied to strengthen object contours, reconnect fragmented regions, or compensate for over-erosion. Dilation is frequently used in combination with erosion to refine binary masks and improve their structural consistency.

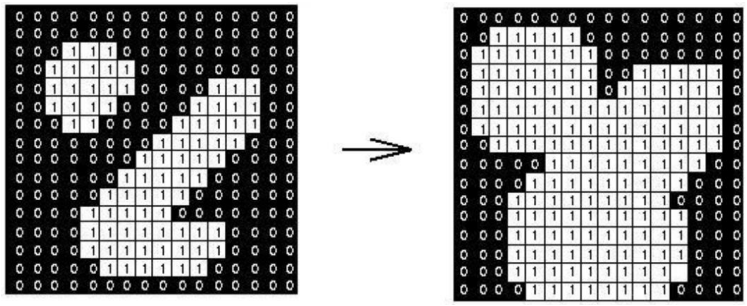

Figure 10: Example of dilation applied on a binary mask

4.1.4 The YOLO framework

YOLO, short for "You Only Look Once," is a family of real-time object detection methods that process an entire image in a single pass. Instead of scanning the image region by region, YOLO uses a convolutional neural network to predict bounding boxes and class labels all at once. The image is divided into a grid, and each grid cell is responsible for generating predictions about objects that appear within its area [14]. This design allows YOLO to achieve fast detection speeds while maintaining competitive accuracy. Over its successive versions, the framework has been refined with improved feature extractors, better loss functions, and more flexible prediction structures, making it widely used in applications requiring efficient and reliable object localization [23]. The latest versions of the model developed by Ultralytics are available in multiple sizes and configurations to balance speed and accuracy. In this thesis, the YOLOv8cls classifier and the YOLOv8s detector are used for silhouette pose validation and anatomical landmark detection respectively.

4.2 Overview of the Pipeline

The architectural graph of the pipeline, the sequence of the checks, and the communication and reliability between the different components

As explained in the Dataset Overview, each patient is photographed from five different angles (−90°, −45°, 0°, 45°, and 90°). The images taken at opposite angles are symmetrical, which means that they follow the same rules and undergo the same checks. For example, a 45° image has the same expected structure as a vertically mirrored −45° image. For this reason, three separate pipelines were created to handle the five angles used during screening.

The pipeline follows a sequential flow, with each check depending on the accuracy of the ones that come before it. The overall structure is shown in Figure 11. If a check determines the image is invalid, no further checks are conducted. Several of the checks are shared across all three pipelines, with the main differences being the thresholds used. Other checks are specific to individual pipelines, but the general logic remains the same.

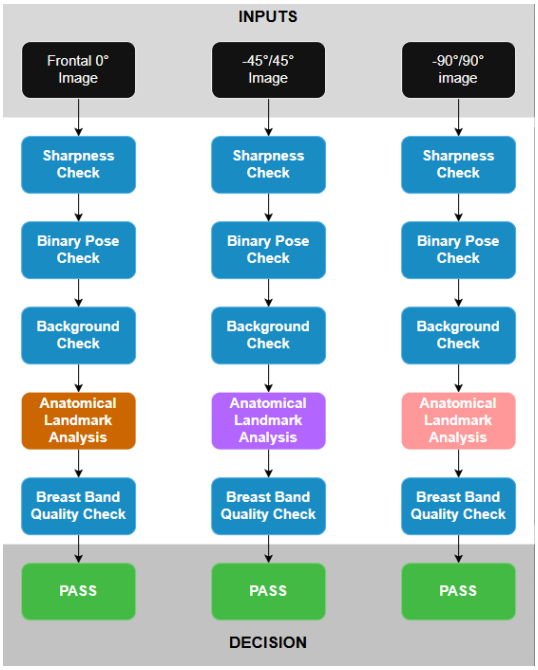

Figure 11: Pipelines Diagram, algorithms in blue are shared between the 3 pipelines, while different colored algorithms are unique to each angle

4.3 Sharpness Check

The first step of the pipeline is to determine whether the image is sufficiently sharp and in focus. To detect blur, the Laplacian operator is applied to the grayscale image to get a mapping of the rate that intensities change. This mapping essentially highlights areas that include edges and fine details. If the image is sharp, these changes are strong and the Laplacian response varies significantly across the pixels. When the image is blurry. The edges are weaker and the Laplacian output becomes more uniform.

To enhance this behaviour, the variance of the Laplacian is then calculated. A high variance indicates a sharp image, while low variance indicates that the image is blurred.

4.3.1 Threshold selection

The Laplacian variance was calculated for all images and the histograms of their Laplacian variance is shown in Figure 12. After examining the histograms, a minimum Laplacian

variance threshold of 10.0 for Frontal images, 5.0 for 45° images, and 7.0 for 90° images was chosen. After this check was rerun on all images with the thresholds mentioned and the images were split into sharp and blurry subfolders, a visual inspection confirmed that these thresholds were well set for this task.

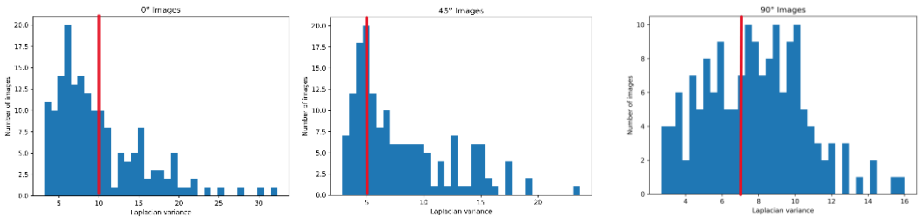

Figure 12: The Laplacian variance histograms and the selected thresholds

4.4 Binary Pose Check

After an image passes the sharpness test, the next step is to verify that the patient is holding the correct pose. Since the original dataset contains almost exclusively valid poses, a separate model was trained to recognize the silhouette of a correct or incorrect stance. This model operates on binary masks rather than thermal intensity values, which allows the classification to rely purely on body shape and outline.

4.4.1 Creating the body mask

The grayscale image is first converted into a binary mask using Otsu's thresholding method. This separates the body from the background by assigning high intensity (hot) pixels to the foreground (white) and lower intensity (cold) pixels to the background (black). Once the mask is created, a small dilation is applied to smooth out irregularities along the silhouette and remove minor gaps, and we then check that only a single white element exists in the mask, and that it is connected to the image's boundaries. The resulting 640 x 480 mask is then padded with black pixels to form a 640 x 640 square image, which matches the input size expected by the YOLOv8cls models. An example is shown in Figure 13.

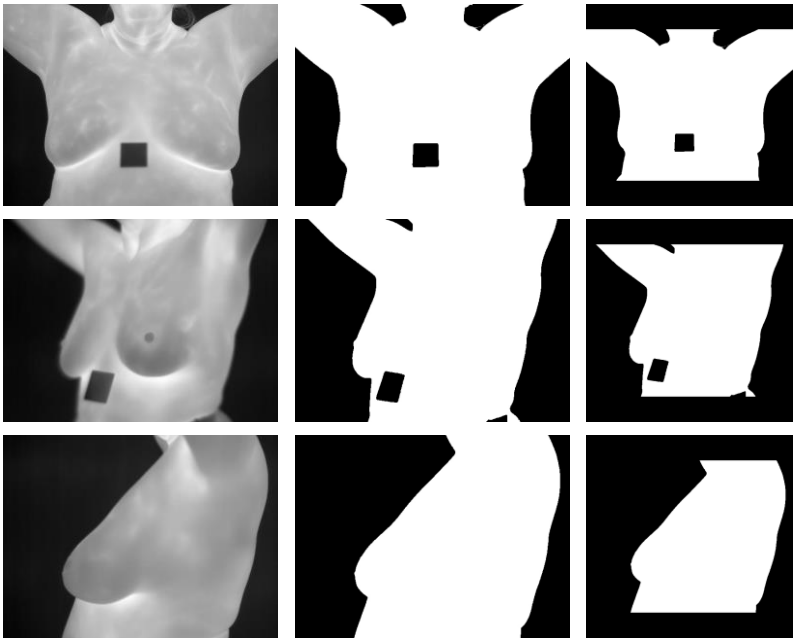

Figure 13: Binary mask creation and padding

4.4.2 Checking silhouette shape

Three different YOLOv8cls models were trained to detect valid and invalid poses for each angle. The padded binary body mask is then passed to its designated YOLOv8cls model, which classifies the pose as either valid or invalid. The classifier is trained to recognize the expected screening posture and to distinguish it from incorrect arm positions, incomplete silhouettes, and other irregular or deformed masks. Examples of invalid body masks are the models are able to classify are shown in Figure 14.

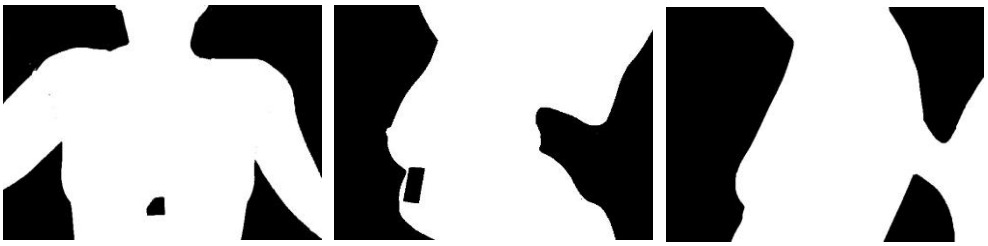

Figure 14: Incorrect and irregular masks the models are able to classify

4.5 Background Quality Check

This check aims to detect any faint heat signatures or noise present in the background of an image. In particular, it identifies artefacts that produce a weak thermal response, warm

enough to appear in the grayscale image, but not warm enough to be included in the foreground during binary thresholding. Because these artefacts fall into the “black” region of the binary body mask, they remain hidden in the silhouette but are still visible in the original thermal image. The purpose of this step is to ensure that the background is free of such unwanted thermal activity before the image proceeds further in the pipeline.

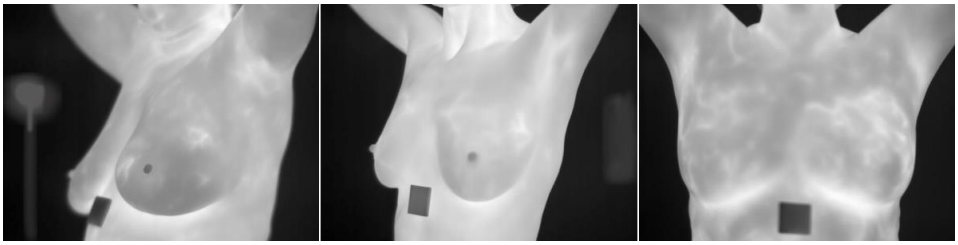

Figure 15: Examples of images with faint thermal objects, thermal noise and clean backgrounds

4.5.1 The Body mask

The mask used to isolate the body is generated in the same way as in the Binary Pose check. Once the body mask is obtained, it is inverted so that the background becomes the highlighted region instead of the torso. A small dilation is then applied to create a margin between the patient’s outline and the background. This buffer helps avoid picking up noise or small artefacts that may occur along the boundary of the silhouette.

Figure 16: Illustrated the original image, the binary mask highlighting the body, and the flipped and eroded mask highlighting the background

4.5.2 Laplacian on background region

The Laplacian operator is then applied to the segmented background to detect if the existence of edges or any random speckle noise is present. The variance of the Laplacian response is then calculated, with a maximum threshold of 35. If the background exceeds that threshold the background is deemed noisy and the image fails.

4.5.3 Segmentation of the background in blocks and statistical metrics

After the background passes the Laplacian check, it is divided into blocks of 8 x 8 pixels. For each block, the mean of the pixel intensities is computed to ensure that no faint or blurred artefacts remain in areas that do not contain edges. A maximum threshold of 60 is used for the mean. If any block exceeds this limit, the background is considered inconsistent and the image fails the check.

4.6 Anatomical Landmark Analysis

At this stage of the pipeline, an image is assumed to be sharp, to contain only a single patient holding a correct pose, and to have a clean background. The next step is to detect the key anatomical landmarks, such as the breasts, armpits, and nipples, and evaluate whether their geometry falls within acceptable limits. The specific landmarks that should appear, as well as their expected arrangement, differ between the three viewing angles, so separate versions of this check were implemented for each angle.

4.6.1 Frontal - 0° images

4.6.1.1 YOLO landmark detector

A YOLOv8s detector model was trained to detect breasts, armpits and nipples in a frontal thermal image using the labeled dataset explained in the Preprocessing section. The three classes the model detects are breast, armpit and nipple. More details of the models training are shown in the Results and Evaluation section.

4.6.1.2 Breast detection

The model detects both breasts and labels them under the single class “breast”. Only detections with a confidence of at least 0.8 are considered valid candidates. From these, the detection whose center lies on the right side of the image’s vertical midline and has the highest confidence is selected as the right breast. The left breast is chosen in the same way, using detections whose centers fall on the left side of the midline.

4.6.1.3 Armpit detection

The armpits are identified in a similar way, but with a lower confidence threshold of 0.4. This reduced threshold is necessary because armpits typically do not form clear edges in thermal images. Instead, the detection relies more on their characteristic thermal pattern than on distinct structural boundaries.

4.6.1.4 Nipple detection

Once the left and right breasts have been selected, all nipple detections with a confidence above 0.5 are taken as candidates. The right nipple is chosen as the highest-confidence detection located within the right breast's bounding box, and the left nipple is selected in the same way. Although nipple detections can help assess the patient's geometry, their absence is not treated as an error. Some patients may not have nipples due to surgery, or the nipples may simply not be visible in thermal images, so missing detections cannot be used as a criterion for invalidating an image. In such cases, virtual nipples are generated instead.

4.6.1.4.1 Single nipple detection

If only one of the two nipples is detected, a virtual nipple is generated for the opposite breast. The position of the detected nipple is first expressed in terms of its relative coordinates within the corresponding breast bounding box. These normalized coordinates are then mirrored vertically onto the other breast's bounding box. In this way, the virtual nipple becomes the symmetrical counterpart of the real one, based on the geometry of the two breast regions.

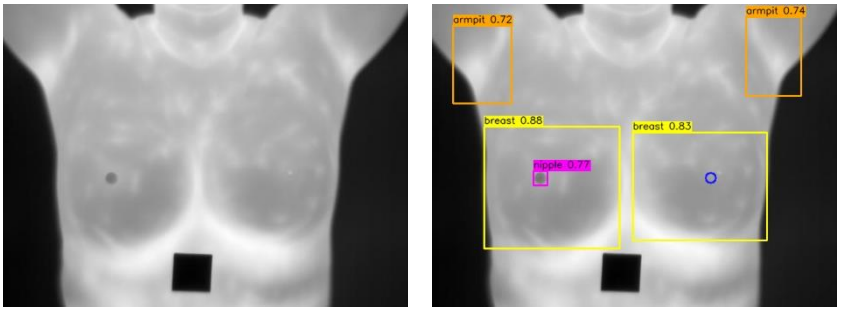

Figure 17: Single nipple detection and virtual nipple generation

4.6.1.4.2 No nipple detections

If no nipples are detected in the breast regions, then two virtual nipples are created for each breast. Each virtual nipple is placed slightly below its breast's bounding box center.

$$VN_x = BB_{cx}$$
$$VN_y = BB_{cy} - BB_h * 0.1$$

Where:

$VN_x -$ *Virtual Nipple x coordinates*

$$VN_y - Virtual\ Nipple\ y\ coordinates$$

$$BB_{cx} - Breast\ Box\ center\ x\ coordinates$$

$$BB_{cy} - Breast\ Box\ center\ y\ coordinates$$

$$BB_h - Breast\ Box\ height$$

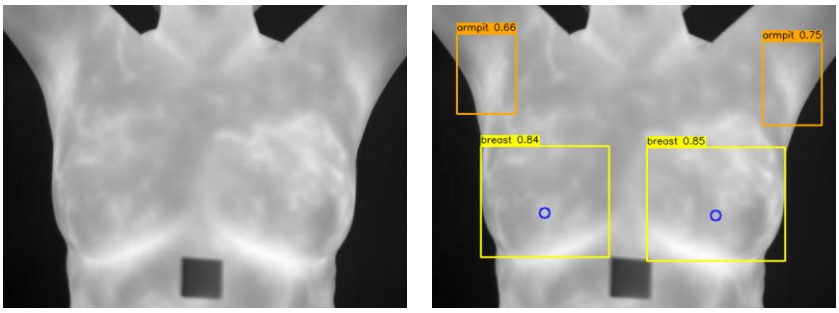

Figure 18: No nipples detected and two virtual nipples generated

4.6.1.5 Landmark geometry

Once all anatomical landmarks have been detected, their relative positions within the image are evaluated. Detections are not allowed to lie too close to the image borders, the armpits must appear above the breasts, and the bounding box sizes must fall within predefined minimum and maximum limits. In addition, the aspect ratios of the bounding boxes are constrained to expected ranges, and excessive size differences between corresponding left and right landmarks are not permitted. After these positional checks are completed, the overall geometry of the landmarks is described using the following metrics:

- Breast distance to image width ratio
- Armpit distance to image width ratio
- Armpits distance to Breasts distance ratio
- Nipple midline point offset (x-axis)
- Armpit midline point offset (x-axis)
- Nipple to armpit midpoint offset (x-axis)
- Nipple angle
- Armpit angle
- Nipples and armpits angle difference

4.6.1.5.1 Breast distance to image ratio

For this metric, the horizontal distance between the centers of the two breast bounding boxes is divided by the image width. This value reflects how close the patient is to the camera. If a patient is standing closer, the breasts occupy a larger portion of the image, so the normalized distance approaches values near 0.6. Conversely, if the patient is positioned farther from the camera, the breasts appear smaller and the distance between their centers represents a smaller fraction of the image width, often around 0.4.

$$BIR = \frac{RB_{cx} - LB_{cx}}{I_w}$$

Where:

$$BIR - Breast\ distance\ to\ Image\ width\ Ratio$$
$$RB_{cx} - Right\ Breast\ center\ x\ coordinates$$
$$LB_{cx} - Left\ Breast\ center\ x\ coordinates$$
$$I_w - Image\ width$$

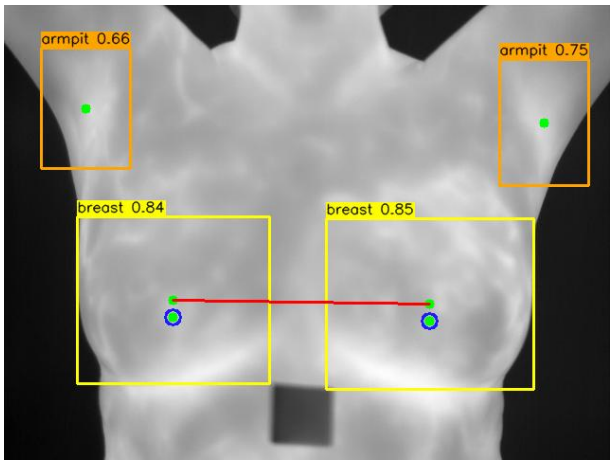

Figure 19: Breast distance line shown in red

4.6.1.5.2 Armpit distance to image ratio

Similarly to the breast distance metric, the horizontal distance between the centers of the two armpit bounding boxes is divided by the image width. This measurement also reflects how far

the patient is standing from the camera, since the armpits appear closer together or farther apart depending on the patient's distance.

$$AIR = \frac{RA_{cx} - LA_{cx}}{I_w}$$

Where:

$$AIR - \ Armpit\ distance\ to\ Image\ width\ Ratio$$
$$RA_{cx} - Right\ Armpit\ center\ x\ coordinates$$
$$LA_{cx} - Left\ Armpit\ center\ x\ coordinates$$
$$I_w - Image\ width$$

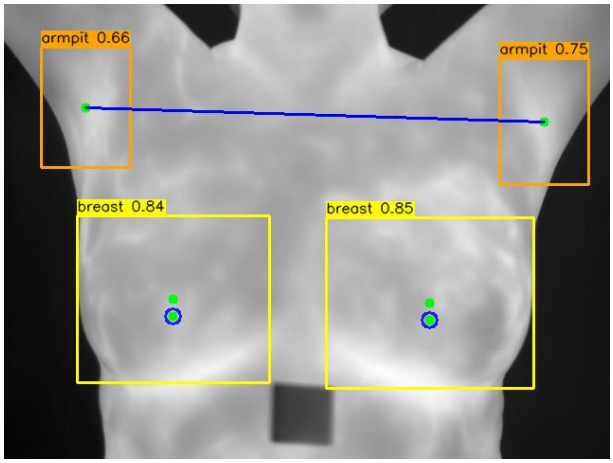

Figure 20: Armpit distance line shown in blue

4.6.1.5.3 Armpits to Breasts distance ratio

This metric is calculated by dividing the distance between the armpits by the distance between the breast centers. It provides an indication of the camera's vertical angle relative to the patient. When the camera is positioned at a level, horizontal height, this ratio is typically around 1.2, since the armpits sit slightly wider than the breasts. If the camera is placed higher and angled downward, the armpits appear closer to the camera while the breasts appear farther away, increasing the ratio toward values around 1.5. Conversely, if the camera is positioned lower and angled upward, the armpits appear farther away and the breasts appear closer, bringing the ratio down toward 1.0.

$$ABR = \frac{AIR}{BIR}$$

Where:

$$ABR - Armpits\ distance\ to\ Breasts\ distance\ ratio$$
$$AIR - Armpit\ distance\ to\ Image\ width\ Ratio$$
$$BIR - Breast\ distance\ to\ Image\ width\ Ratio$$

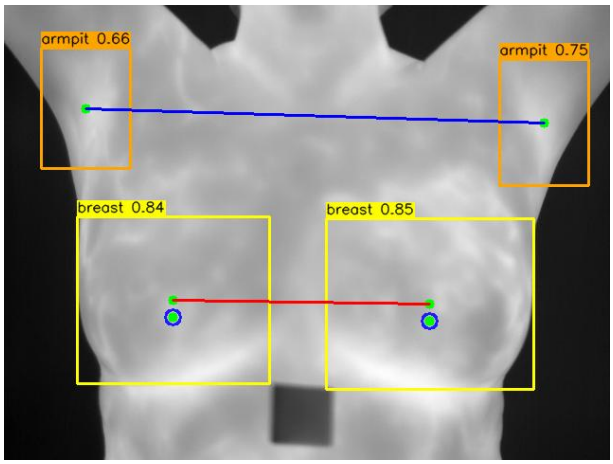

Figure 21: Armpit distance shown in blue and breast distance in red

4.6.1.5.4 Nipple midline point offset

This metric first calculates the midpoint between thenipples. The offset of this midpoint from the image's vertical midpoint is then measured to determine how well centered the breasts are within the image frame.

$$NMP = \frac{RN_{cx} + LN_{cx}}{2}$$

$$NMP_{offset} = abs\left(NMP - \frac{I_w}{2}\right)$$

Where:

$$NMP - Nipple\ centers\ Midline\ Point$$
$$RN_{cx} - Right\ Nipple\ center\ x\ coordinates$$
$$LN_{cx} - Left\ Nipple\ center\ x\ coordinates$$
$$I_w - Image\ width$$

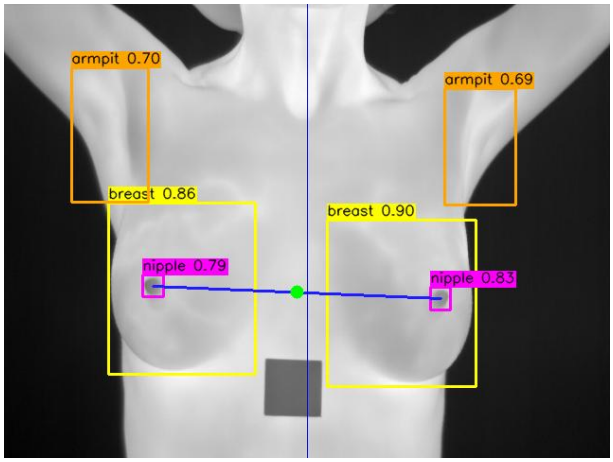

Figure 22: Nipple midpoint shown in red and image midline in blue

4.6.1.5.5 Armpit centers midline point offset

Similarly to the Breast center midline offset, this metric first calculates the midpoint between the centers of the two armpits. The offset of this midpoint from the image's vertical midpoint is then measured to determine how well centered the armpits are within the image frame.

$$AMP = \frac{RA_{cx} + LA_{cx}}{2}$$

$$AMP_{offset} = abs\left(AMP - \frac{I_w}{2}\right)$$

Where:

$$AMP - Breast\ centers\ Midline\ Point$$
$$RA_{cx} - Right\ Armpit\ center\ x\ coordinates$$
$$LA_{cx} - Left\ Armpit\ center\ x\ coordinates$$
$$I_w - Image\ width$$

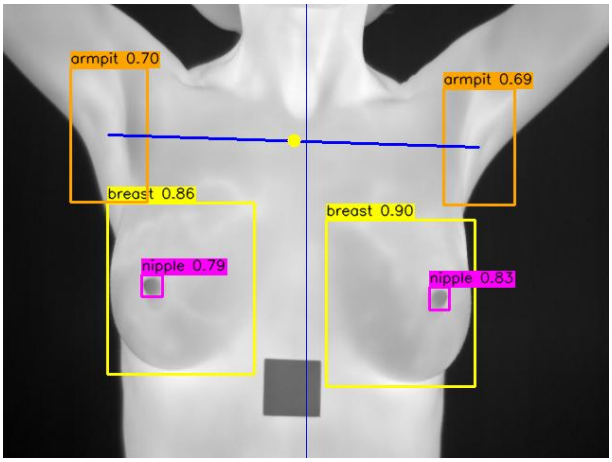

4.6.1.5.6 Nipple to Armpit midpoint difference

This metric computes the horizontal distance between the midpoint of the two nipples and the midpoint of the two armpits. Under correct positioning, these two midpoints are expected to be vertically aligned. A noticeable horizontal offset between them indicates a rotation of the torso relative to the camera, suggesting that the patient may be slightly turned or twisted during image capture. This measure therefore helps identify cases where the body is not facing the camera directly, even if individual landmarks appear correctly detected.

$$NAMD = abs(NMP - AMP)$$

Where:

$$NAMD - Nipple\ and\ Armpit\ Midpoints\ Distance$$
$$NMP - Nipple\ centers\ Midline\ Point$$
$$AMP - Armpit\ centers\ Midline\ Point$$

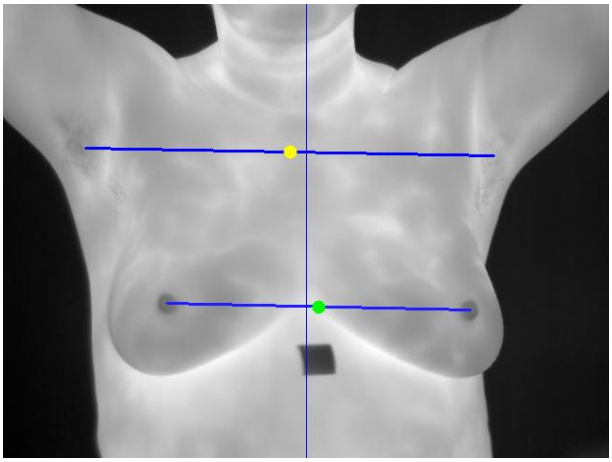

Figure 23: Midpoints of armpits and nipples relative to the image's vertical midline

4.6.1.5.7 Nipple angle

This metric computes the angle defined by the two nipple positions. When the breasts are aligned horizontally, the angle is close to zero. A large angle indicates that one side is positioned higher or lower than the other, which reflects a tilt in the patient's posture or in the camera's orientation.

$$\theta_{nip} = arctan2(\Delta_{cy}, \Delta_{cx}) * \frac{180}{\pi}$$

Where:

$$\theta_{nip} - Angle\ of\ the\ nipples\ in\ degrees$$
$$\Delta_{cx} - Difference\ of\ the\ nipples'\ x\ coordinates$$
$$\Delta_{cy} - Difference\ of\ the\ nipples'\ y\ coordinates$$

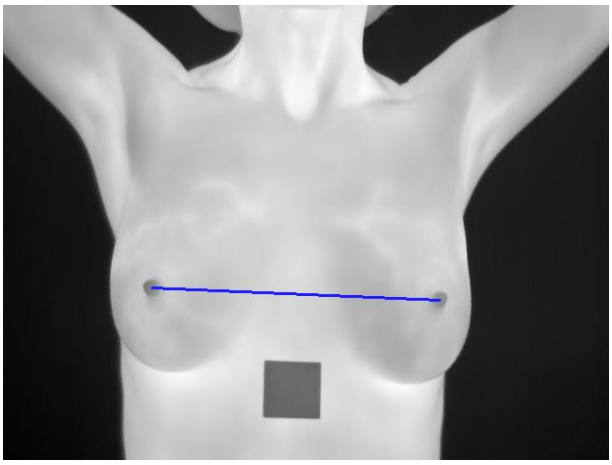

Figure 24: Nipple angle line shown in blue

4.6.1.5.8 Armpit angle

This metric computes the angle defined by the two armpit positions. Similar to the nipple angle, it provides an indication of the patient's tilt or the camera's vertical orientation.

$$\theta_{armp} = arctan2(\Delta_{cy}, \Delta_{cx}) * \frac{180}{\pi}$$

Where:

$$\theta_{armp} - Angle\ of\ the\ armpits\ in\ degrees$$

$$\Delta_{cx} - Difference\ if\ the\ armpits'\ x\ coordinates$$
$$\Delta_{cy} - Difference\ if\ the\ armpits'\ y\ coordinates$$

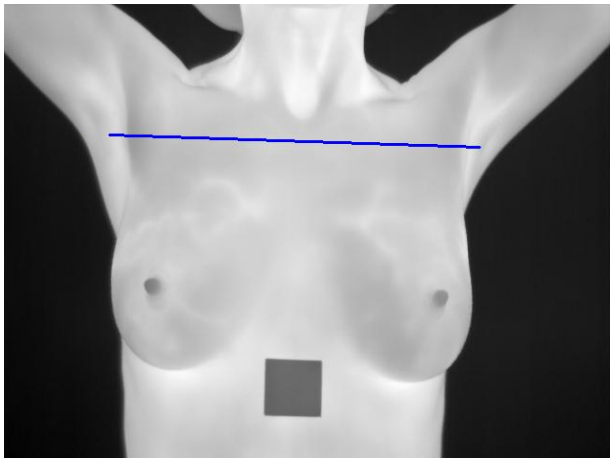

Figure 25: Armpit angle line shown in blue

4.6.1.5.9 Nipples and Armpits angle difference

This metric compares the angle defined by the armpits with the angle defined by the nipples. Rather than describing a global tilt of the body, it captures differences in orientation between the upper torso and the breast region. In some cases, a patient may lean their shoulders toward one side while the chest and breasts remain oriented differently, or vice versa. Such asymmetries can arise from uneven posture, slight body rotation, or compensatory arm positioning during image capture. A large difference between the armpit and nipple angles therefore indicates an inconsistent body alignment, even if each angle on its own appears acceptable.

$$\Delta\theta_{nip,armp} = abs(\theta_{nip} - \theta_{armp})$$

Where:

$$\Delta\theta_{nip,armp} - Nipple\ and\ Armipt\ angle\ difference$$
$$\theta_{nip} - Nipple\ angle$$
$$\theta_{armp} - Armpit\ angle$$

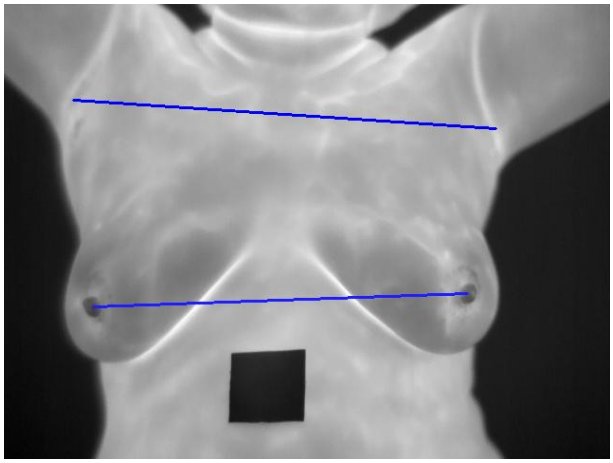

Figure 26: Example of a patient with a relatively big nipple to armpit angle difference

4.6.1.5.10 General geometry using the metrics

These metrics together are sufficient to describe the relative geometry of the patient's anatomical landmarks. By applying thresholds to each metric, the pipeline limits the amount of variability that can be accepted across images from different patients. This normalization is particularly important because patients with different body sizes and shapes naturally project their anatomical landmarks to different positions in the image, even when standing at the same physical distance from the camera. As a result, patients with larger or smaller body frames must adjust their stance and positioning so that their anatomical landmarks fall within the expected geometric ranges. Enforcing these constraints ensures that the images are comparable and suitable for consistent downstream analysis.

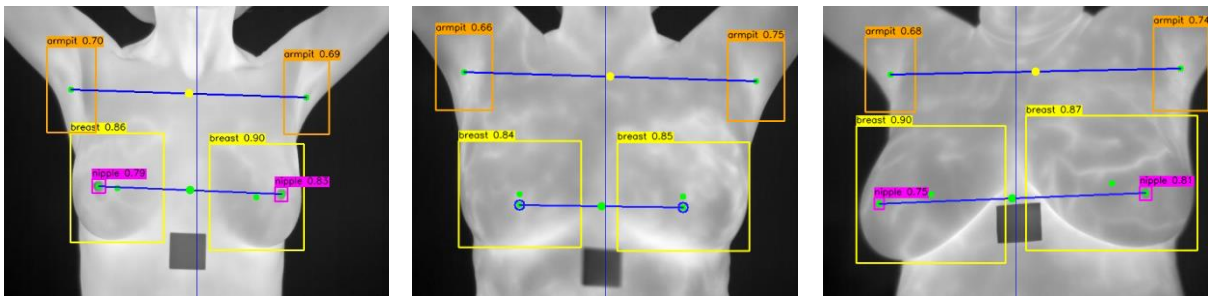

Figure 27: Images with all metrics illustrated

4.6.2 45° images

4.6.2.1 YOLOv8s landmark detector

A YOLOv8s detector model was trained to detect breasts, armpits and nipples in a 45° thermal image using the labeled 45° dataset explained in the Preprocessing section. The three classes the model detects are left breast, right breast, armpit and nipple. More details of the models training are shown in the Results and Evaluation section.

4.6.2.2 Breast detection

For the 45° views, the model predicts the left and right breasts as separate classes and assigns a distinct label to each. This distinction is necessary because the breast farther from the camera is typically visible in side profile, while the breast closer to the camera appears more diagonally and occupies a larger area in the image. Differentiating between the left and right breast therefore provides important information about the patient's orientation and helps determine the direction in which the patient is facing during image acquisition.

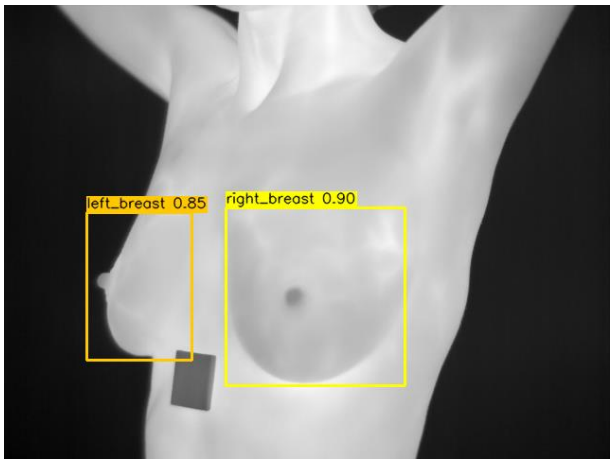

Figure 28: Example of left and right breast detections

4.6.2.3 Armpit detection

In contrast to the frontal views, only one armpit is expected to be visible in a 45° image. The detected armpit is selected based on a minimum confidence threshold, and only detections exceeding this threshold are considered as candidates. The candidate with the highest confidence score is selected.

4.6.2.4 Nipple detection

In 45° screenings, both nipples are ideally visible. However, as with frontal images, their presence is not guaranteed. For this reason, a similar strategy used in the frontal case is

applied: when one or both nipples are not detected, virtual nipples are generated based on the available anatomical information.

4.6.2.4.1 Real nipple detection

If a nipple is detected with sufficient confidence inside a breast bounding box, it is considered as a candidate for that breast, and the detection with the highest confidence score is selected.

4.6.2.4.2 No nipple detection

If no nipple detections inside a breast bounding box surpass the minimum confidence threshold, a virtual nipple is generated for that breast. The position of the virtual nipple is slightly to the left of the breast's bounding box center.

$$VN_x = BB_{cx} - 0.25 * BB_w$$
$$VN_y = BB_{cy}$$

Where:

$$VN_x - Virtual\ Nipple\ x\ coordinates$$
$$VN_y - Virtual\ Nipple\ y\ coordinates$$
$$BB_{cx} - Breast\ Box\ center\ x\ coordinates$$
$$BB_{cy} - Breast\ Box\ center\ y\ coordinates$$
$$BB_w - Breast\ Box\ width$$

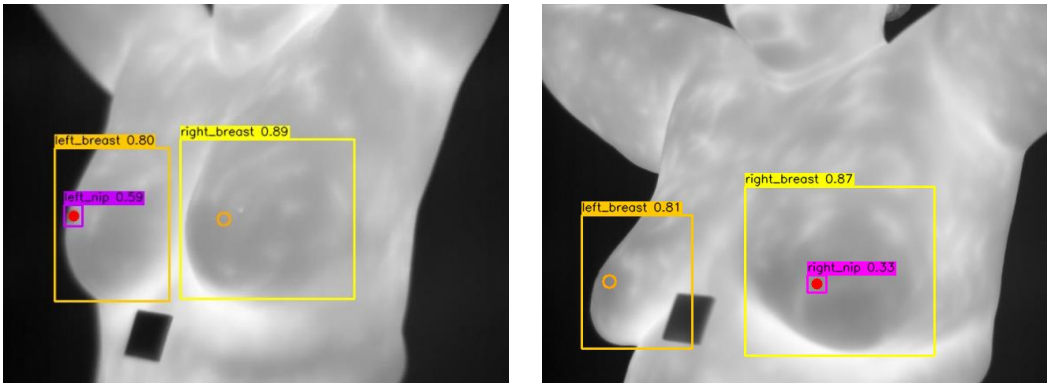

Figure 29: Examples of a right virtual nipple and a left virtual nipple

4.6.2.5 Anatomical landmark geometry

Once all required anatomical landmarks have been detected and the most reliable candidates have been selected, their spatial arrangement within the image is evaluated. As a first step,

each landmark is checked to ensure that it is not positioned too close to the image borders, which could indicate improper framing. The right breast is expected to appear roughly centered horizontally and should not lie too close to the lower edge of the image, as this would suggest incorrect camera placement or patient positioning. In addition, the armpit is expected to appear sufficiently above and to the right of the right (closest to the camera) breast, see Figure 30. If the armpit is detected to the left of the right breast, this indicates that the patient is facing the wrong direction relative to the camera, and the image is considered invalid, see Figure 31.

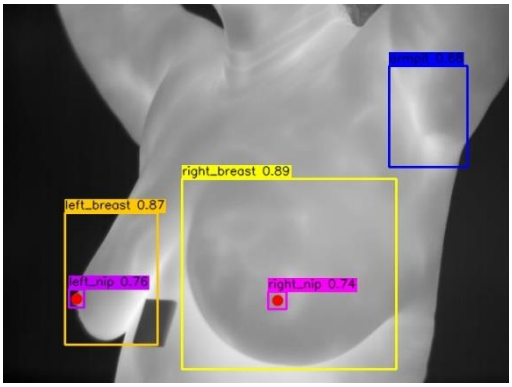

Figure 30: Example of a correct orientation, the armpit is sufficiently above and to the right of the "right breast"

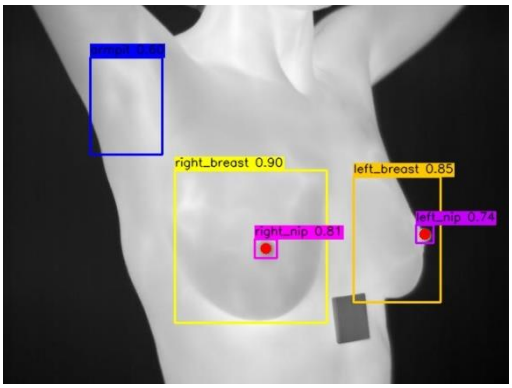

Figure 31: Example of incorrect orientation, the armpit is above and towards the left of the "right breast"

After the positioning of each landmark is assessed, the detections are then used to compute the following metrics:

- Nipple angle
- Nipple distance to image width ratio (x-axis)

4.6.2.5.1 Nipple angle

This metric computes the angle formed by the two nipple positions. The resulting angle reflects the relative height and tilt between the camera and the breast region. When the angle is close to zero, the line connecting the nipples is approximately horizontal, indicating that the camera is positioned at the same height as the breasts, an example is shown in Figure 32. If the angle exceeds +20°, the camera is likely positioned above the breasts and angled downward, an example is shown in Figure 33. Conversely, if the angle falls below −10°, the camera is positioned below the breast level and angled upward.

$$\theta_{nip} = arctan2(\Delta_{cy}, \Delta_{cx}) * \frac{180}{\pi}$$

Where:

$$\theta_{nip} - Angle\ of\ the\ nipples\ in\ degrees$$
$$\Delta_{cx} - Difference\ of\ the\ two\ nipples'\ x\ coordinates$$
$$\Delta_{cy} - Difference\ of\ the\ two\ nipples'\ y\ coordinates$$

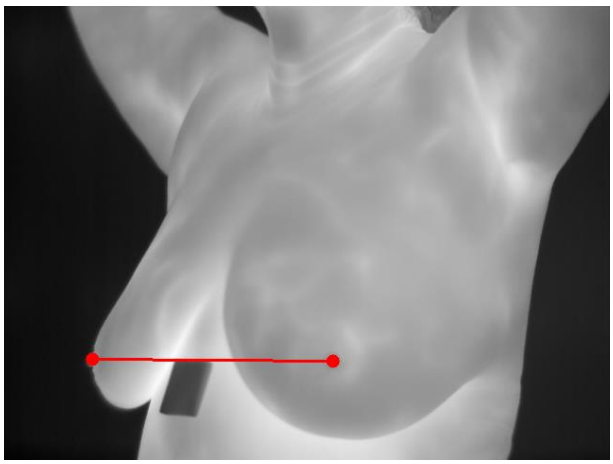

Figure 32: Example of a horizontal nipple line

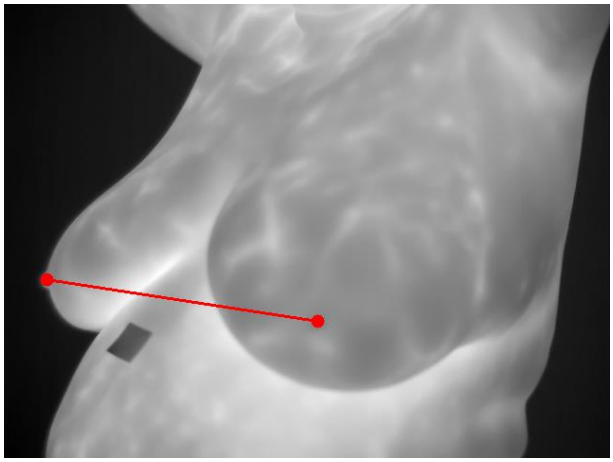

Figure 33: Example of a positive nipple angle, showing a slight top-down view of the breasts

4.6.2.5.2 Nipple distance to image width ratio

This metric computes the horizontal distance between the two nipple positions and normalizes it by the image width. The resulting ratio reflects the degree of rotation of the patient's body relative to the camera. A small ratio indicates that the patient is over-rotated, with more of their side facing the camera, an example is shown in Figure 34. A larger ratio suggests that the patient is not rotated enough and is closer to a frontal orientation.

Figure 34: Example of a patient that is over-rotated, the horizontal nipple distance is small relative to the image width

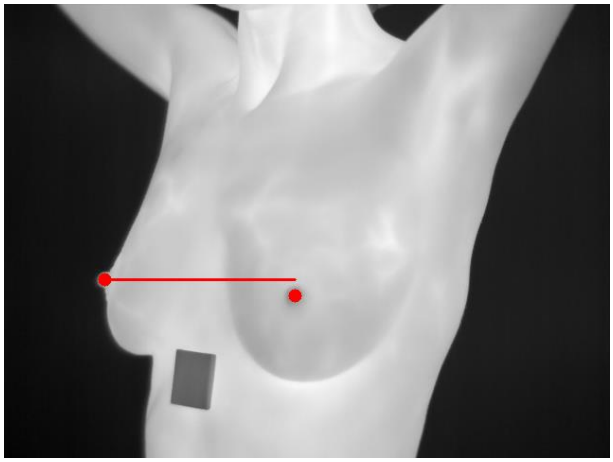

Figure 35: Example of a patient with an acceptable orientation, nipple distance to image width ratio within limits

4.6.2.6 General geometry using the detections and metrics

In 45° screenings, pose validity is determined by both the absolute position of the anatomical landmarks within the image and the geometric metrics computed from them. By constraining where each landmark is allowed to appear, the pipeline ensures that the patient is standing at an appropriate distance from the camera, that no landmarks are cropped or missing, and that the screening is correctly centered on the right breast. The nipple-based metrics are then used to further verify the patient's body orientation, confirming that the rotation is appropriate and that the right breast is properly presented to the camera.

4.6.3 90° images

4.6.3.1 YOLOv8s landmark detector

As with the other viewing angles, a YOLOv8s detector was trained to identify anatomical landmarks in side-profile images. In this case, only a single breast and one armpit are expected to be visible, so nipple detection is not required, as no bilateral distances or angle-based metrics are computed. Additional details regarding the training of this model are presented in the Results and Evaluation section.

4.6.3.2 Breast detection

Any breast detection with a confidence score above the minimum threshold is considered a candidate, and the detection with the highest confidence score is selected. The selected breast's bounding box is then checked to ensure that its size falls within acceptable limits and that its aspect ratio is within the expected range. After these initial checks, the position of the

bounding box center is evaluated to confirm that it lies within an acceptable region of the image. This region is generally centered, with a slight bias toward the bottom left side, and is illustrated in Figure 36. Finally, the bounding box edges are evaluated to ensure that they are not positioned too close to the image borders.

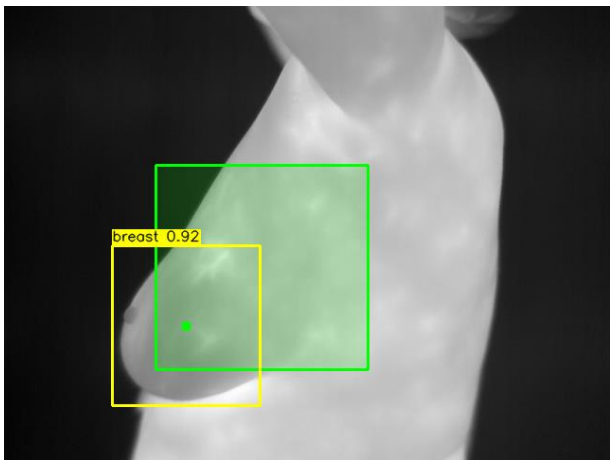

Figure 36: Illustrated breast bounding box, it's center (green dot), and the acceptable region (transparent green box)

4.6.3.3 Nipple detection

Similar to the breast detection process, all armpit detections with a confidence above the minimum threshold are considered candidates, and the detection with the highest confidence score is selected. The selected armpit is then checked to ensure that its center lies within an acceptable region of the image. For side-profile views, this region corresponds to the upper-right quarter of the image frame, as illustrated in Figure 37. Finally, the bounding box edges are evaluated to ensure that they are not positioned too close to the image borders.

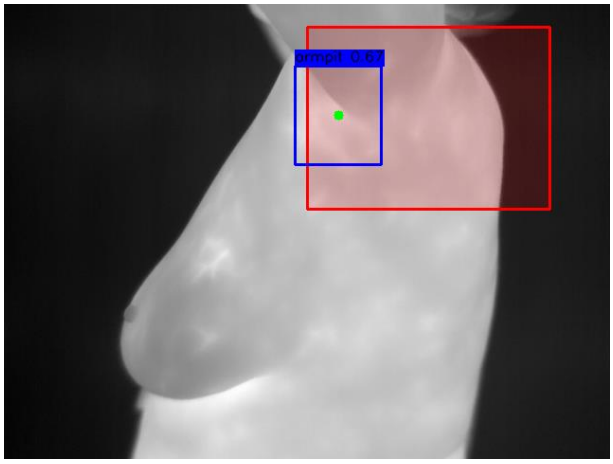

Figure 37: Illustration of armpit bounding box (blue), it's center (green dot), and the acceptable region (red transparent box)

4.6.3.4 Breast to armpit positioning

After both the breast and the armpit have been detected, their relative positions are evaluated. The center of the armpit is required to lie at least 15% of the image height above, and 15% of the image width to the right of, the breast's center. These constraints ensure that the anatomical landmarks follow the expected spatial arrangement and help prevent misalignments caused by incorrect pose or camera orientation.

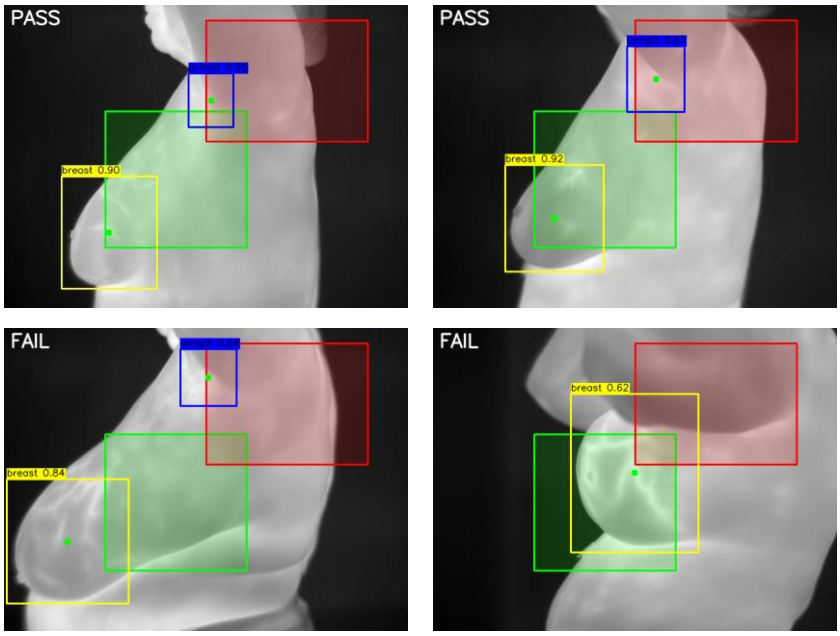

Figure 38: Examples of detections and acceptable regions

4.6.4 Determining valid pose

All metrics presented for the different viewing angles are evaluated against predefined threshold values. By adjusting these thresholds, the strictness of the pose validation process can be controlled, allowing the pipeline to be either more permissive or more selective depending on the application requirements. If an image violates any of the thresholds corresponding to its designated viewing angle, it is automatically classified as invalid and rejected from further processing.

4.7 Breast Band Quality Check

At this stage of the pipeline, the image is expected to depict a patient holding a valid pose, with anatomical landmarks located within their expected regions for the given viewing angle. In addition, the background is assumed to be free of thermal noise or artefacts, and the image has already passed the sharpness check. The breast band quality check is the final stage of the sequential pipeline. Its purpose is to assess whether the patient has allowed sufficient time for the chest to cool, thereby enhancing meaningful thermal patterns, and to verify the absence of occlusions such as clothing or large cold regions caused by water, lotions, or rubbing alcohol.

It is important to note that the DMR-IR dataset used in this thesis was originally created to evaluate different patient preparation protocols and their impact on revealing clearer thermal patterns in the breast region. As a result, the dataset contains no images that exhibit serious violations of these protocols, such as insufficient cooling time, the presence of clothing, accessories like jewelry, or pronounced cold spots. To address this limitation and enable the development and evaluation of the breast band quality algorithm, manual image editing was applied to selected images in order to simulate such conditions.

4.7.1 Band Mask Extraction

To allow the algorithm to focus specifically on thermal patterns within the body, a binary mask isolating the patient from the background is generated in a manner similar to the background quality check. The grayscale thermal image is converted into a binary image using Otsu's thresholding method, producing a mask that highlights the body region. To further restrict the mask to the chest area, it is cropped at the top and bottom to remove regions corresponding to the arms and abdomen. A single erosion operation is then applied to slightly shrink the mask, creating a margin between the inner body region and the body edges. The steps involved in creating this mask are illustrated in Figure 39.

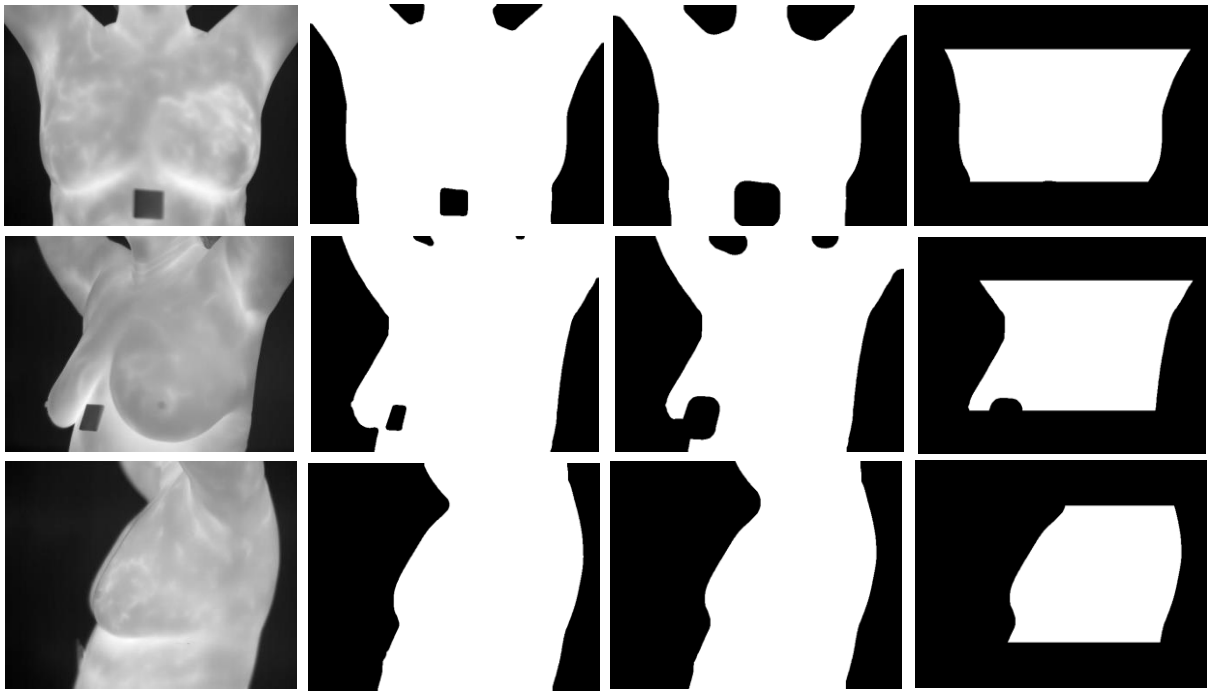

Figure 39: Examples of the original images, body masks, eroded body masks and breast masks

The resulting body mask makes it possible to compute metrics based on the thermal intensities and patterns present in the chest region, which are then used to assess the thermal quality of the breasts.

4.7.2 Coverage Metric

The coverage metric evaluates how much of the expected breast band region is occupied by valid body pixels. After the chest-focused body mask is created, the percentage of body (white) pixels within the breast band area is calculated. This ratio represents how much of the region is effectively covered by the patient's body and contributes meaningful thermal information.

A low coverage value indicates that a significant portion of the breast band is missing or obstructed. This may occur due to occlusions such as clothing, towels, or accessories, as well as large cold regions caused by water, lotions, or rubbing alcohol. In contrast, a high coverage value suggests that the breast area is fully visible and unobstructed. If the coverage falls below a predefined threshold, the image is considered unsuitable for further analysis and fails the breast band quality check.

4.7.3 Symmetry Metrics

Thermal symmetry between the left and right sections of the breast mask is evaluated only for frontal images, where the patient is expected to be facing the camera directly and the body is approximately vertically symmetric. For 45° and 90° views, such symmetry is not expected due to perspective effects, and therefore symmetry-based metrics are not applied.

To assess the symmetry of the frontal breast mask, the mask is divided into left and right components using the vertical midline of the original image. The pixel area of each component is then calculated, and a symmetry ratio is obtained by dividing the larger area by the smaller one. A perfectly symmetric breast mask would produce a ratio close to 1. Values greater than 1.4 indicate significant asymmetry, suggesting uneven coverage or potential occlusions in the breast region.

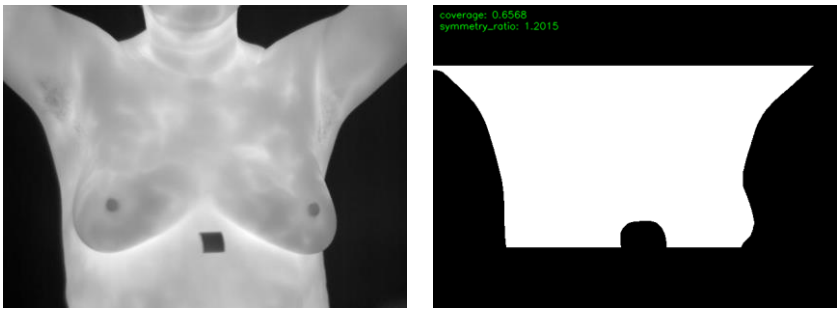

Figure 40: Example of the coverage and symmetry metrics on a frontal image

4.7.4 Intensity Metrics

The intensity-based metrics focus on the thermal activity and patterns present in the chest region. In thermal images, pixel intensity values directly correspond to surface temperature measurements. By computing statistical metrics from these intensities, it becomes possible to assess the patient's body temperature, evaluate the visibility and contrast of thermal features such as blood vessels, and identify colder regions of the chest. Such cold areas may result from insufficient cooling time or from external factors like water, lotions, or other substances, and can negatively affect the quality of the thermal screening.

4.7.4.1 Mean intensity

If a patient has not allowed sufficient time for the chest to cool, the breast region may still exhibit thermal patterns, but the overall pixel intensities will be higher than expected due to elevated surface temperature. Conversely, if the chest appears significantly colder than

anticipated, this may indicate the presence of clothing or the application of liquids on the skin, which can diffuse or suppress the heat emitted by the body.

By calculating the mean intensity of all pixels within the breast mask, an estimate of the patient's surface temperature can be obtained. Applying upper and lower thresholds to this mean value allows the pipeline to define an acceptable temperature range, which helps ensure that only thermally consistent images are passed to the downstream breast cancer classification model.

4.7.4.2 Intensity variance

In addition to maintaining an acceptable average surface temperature, thermal screenings must also display sufficient thermal patterns, such as those associated with blood vessels, in adequate detail. These patterns can be weakened or obscured by patient movement, slight defocusing of the camera, or the presence of liquids on the skin. Assessing these effects is important, as the downstream breast cancer classification model relies heavily on the visibility and quality of such thermal features.

By computing the variance of pixel intensities within the chest region, it is possible to evaluate whether meaningful thermal patterns are present. A high intensity variance indicates well-defined thermal activity, while a low variance suggests a more uniform temperature distribution, which may signal poor image quality.

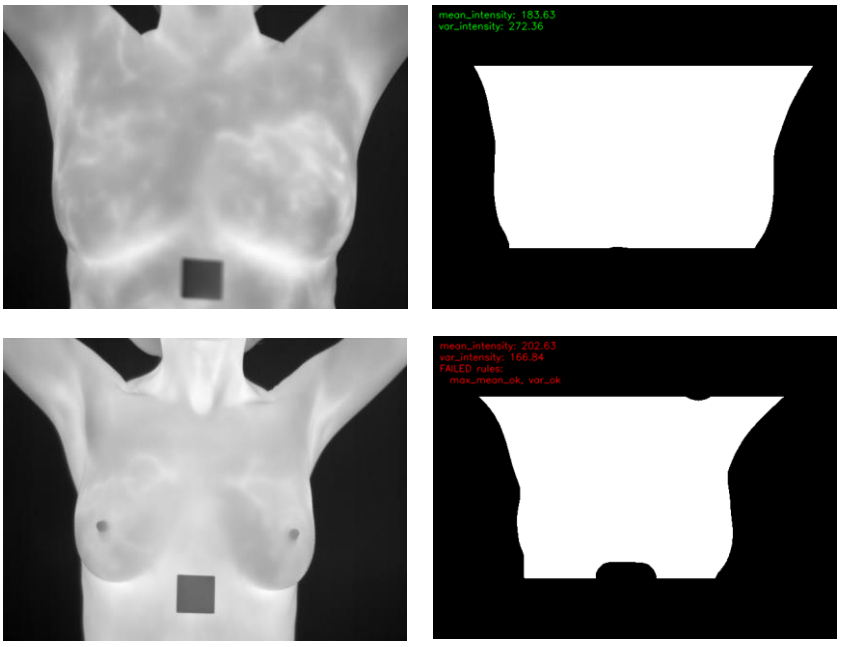

Figure 41: Examples of Intensity mean and variance on frontal images

4.7.5 Occlusion Detection

One important source of error that must be assessed is the presence of occlusions. In the context of thermal imaging, an occlusion refers to any factor that suppresses or blocks meaningful thermal patterns on the chest surface. Occlusions may occur when a patient wears tight or thin clothing that has adapted to body temperature, allowing the outline of the breasts to remain visible while obscuring finer thermal details such as blood vessel patterns. Similarly, the application of liquids, such as water, lotions, or rubbing alcohol, to parts of the chest can locally reduce surface temperature, causing these regions to appear significantly colder than the surrounding tissue. Such effects can distort the true thermal distribution of the breasts and interfere with reliable analysis, making occlusion detection a necessary component of the quality assessment pipeline.

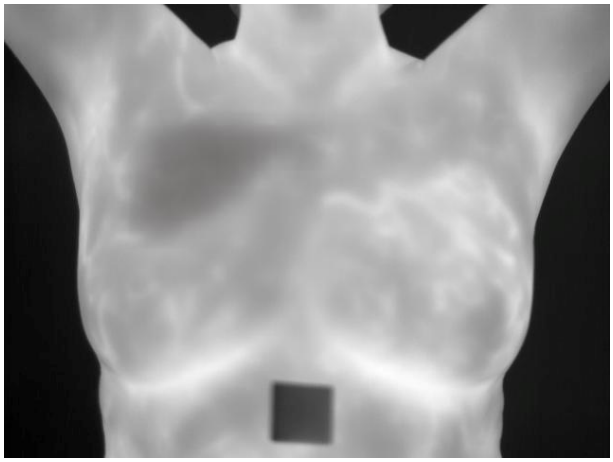

Figure 42: An occlusion above the left breast, manually edited on the image

4.7.5.1 Cold pixel selection

Cold pixels are identified by analyzing deviations from the overall thermal distribution of the breast band region. After the breast band mask is applied, the mean intensity μ and standard deviation σ of all pixels within the mask are computed. A pixel is classified as cold if its intensity value falls significantly below the average thermal level of the region. Specifically, pixels with intensity values lower than $\mu - \kappa * \sigma$ are selected as cold candidates, where κ is a predefined constant used to adjust the relative threshold of what is considered a cold pixel.

This relative thresholding approach allows cold pixels to be detected independently of absolute temperature values, making the method robust to variations in overall body

temperature and imaging conditions. By defining cold pixels in relation to the image's own intensity distribution, the algorithm focuses on identifying localized temperature drops that are more likely to be caused by occlusions or external interference rather than normal physiological variation.

4.7.5.2 Cold pixel clustering to determine occlusions

Once the intensity threshold for cold pixels is established, all pixels with values below this threshold are included in a binary cold-pixel mask. This mask is then decomposed into elements, where each element represents a cluster of cold pixels that are connected to each other, shown in Figure 43. The area of each cluster is computed, and the largest one is selected for evaluation. If the area of the largest cold cluster exceeds a predetermined fraction of the area of pixels in the original breast mask, the cluster is considered an occlusion, and the image fails the breast band quality check.

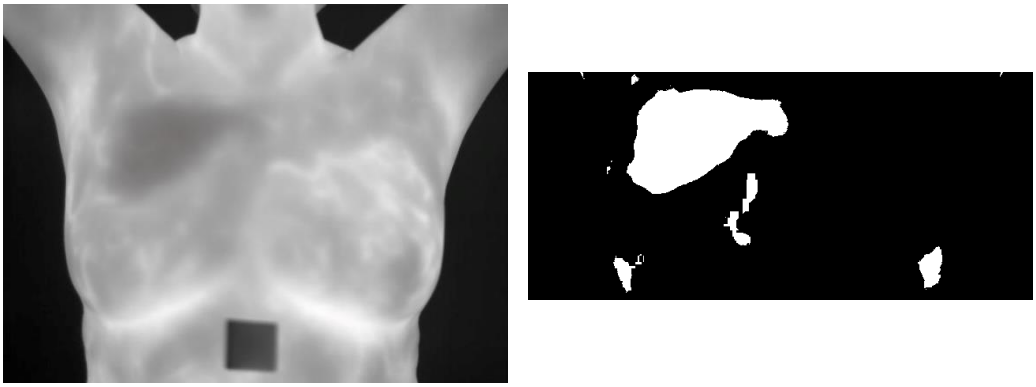

Figure 43: Example of the mask containing the cold pixel clusters

5 Results and Evaluation

5.1 YOLO models metrics and results

5.1.1 Frontal - 0° Models

5.1.1.1 Binary pose classifier

The YOLOv8cls model was trained for 40 epochs, with weights saved every two epochs. The training and validation metrics are presented in Figure 44. The lowest validation loss was achieved at epoch 30, and the corresponding weight configuration was therefore selected as the final model. The dataset used for training consisted of 149 binary frontal pose images, including 71 valid and 78 invalid samples. This dataset was split into 80% training (117 images), 10% validation (16 images), and 10% testing (16 images). The model achieved an inference time of 73.1 ms per image.

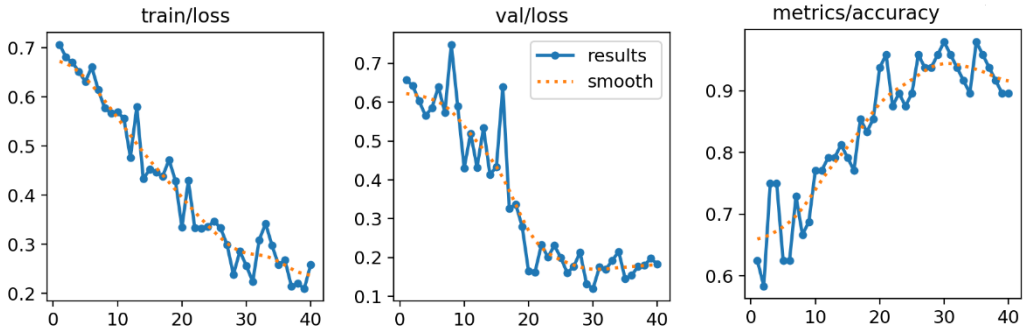

Figure 44: YOLOv8cls binary frontal pose classifier metrics

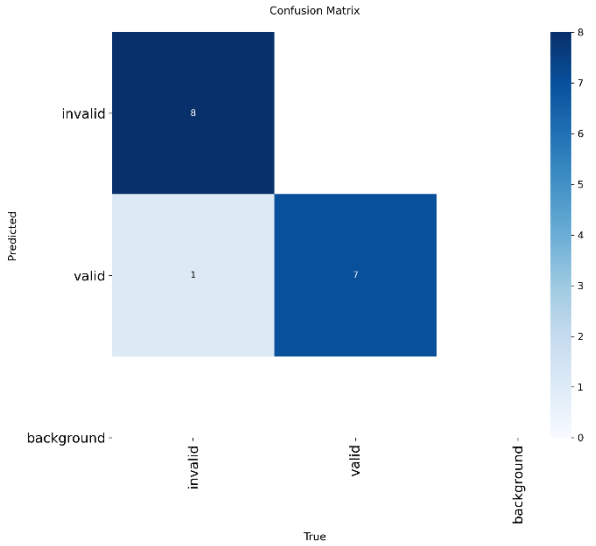

Figure 45: YOLOv8cls binary frontal pose confusion matrix

5.1.1.2 Anatomical landmark detector

The YOLOv8s detector used for frontal anatomical landmark detection was trained for 20 epochs. The training and validation metrics are shown in Figure 46. The dataset consisted of 168 labeled images and was split into 80% training (134 images), 10% validation (16 images), and 10% testing (18 images). The model achieved an inference time of 130.0 ms per image.

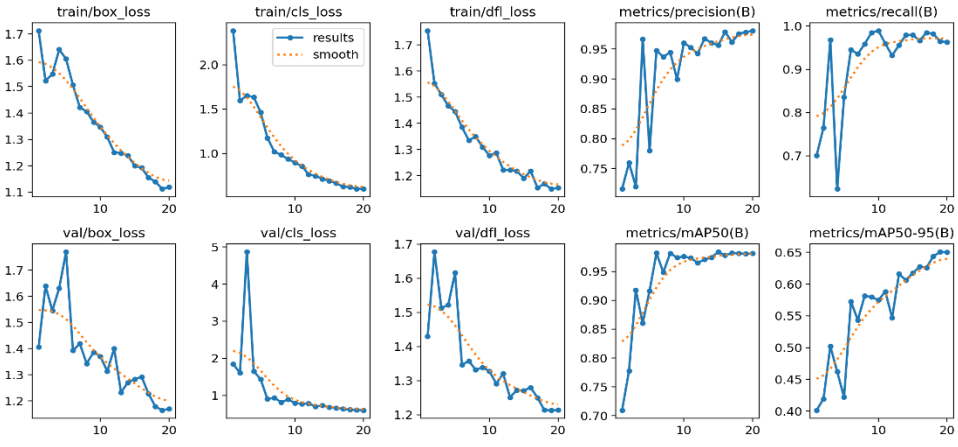

Figure 46: YOLOv8s frontal anatomical landmark detector metrics

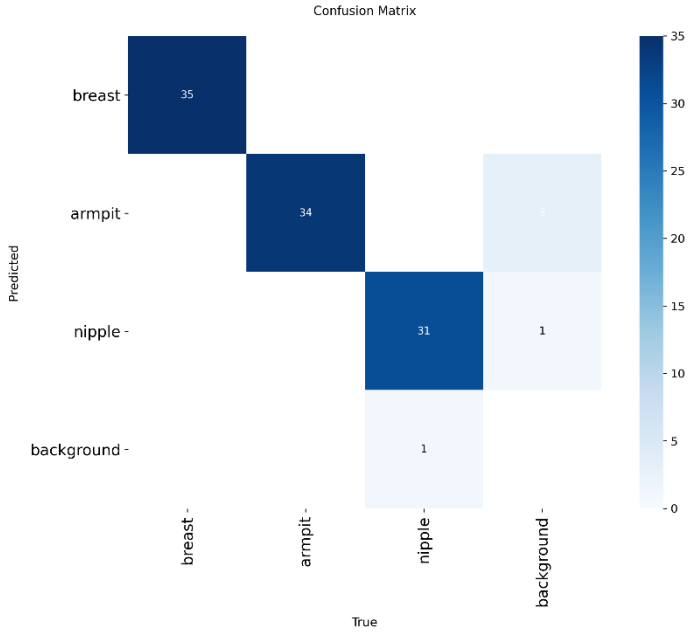

Figure 47: YOLOv8s frontal anatomical landmark detector confusion matrix

5.1.2 45° Models

5.1.2.1 Binary pose classifier

The YOLOv8cls model was trained for 20 epochs. The training and validation metrics are presented in Figure 48. The dataset used for training consisted of 289 binary 45° pose images, including 148 valid and 141 invalid samples. This dataset was split into 70% training (203 images), 15% validation (43 images), and 15% testing (43 images). The model achieved an inference time of 67.4 ms per image.

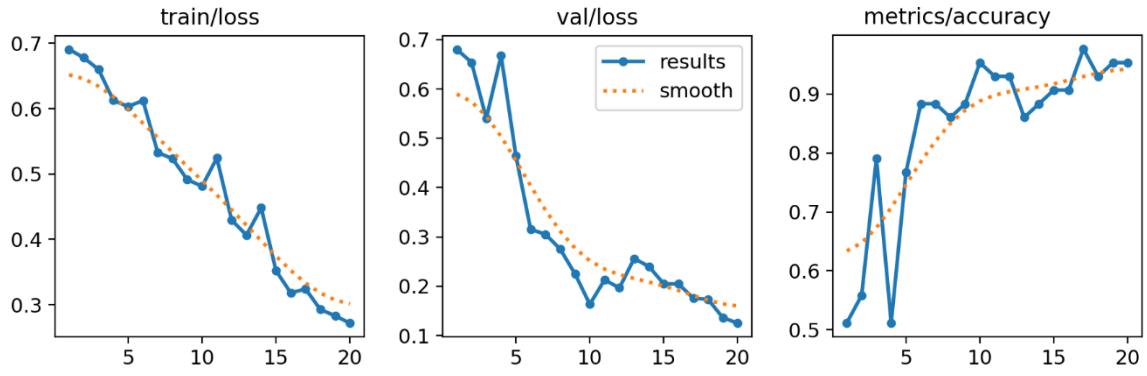

Figure 48: YOLOv8cls 45° binary pose classifier training and validation results

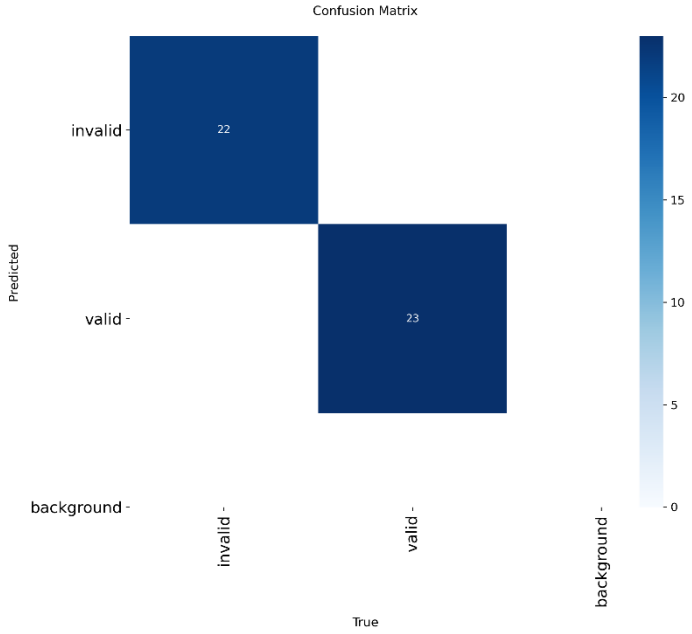

Figure 49: YOLOv8cls 45° binary pose classifier confusion matrix

5.1.2.2 Anatomical landmark detector

The YOLOv8s detector used for 45° anatomical landmark detection was trained for 30 epochs. The training and validation metrics are shown in Figure 50. The dataset consisted of 153 labeled images and was split into 80% training (122 images), 10% validation (15 images), and 10% testing (16 images). The model achieved an inference time of 143.7 ms per image.

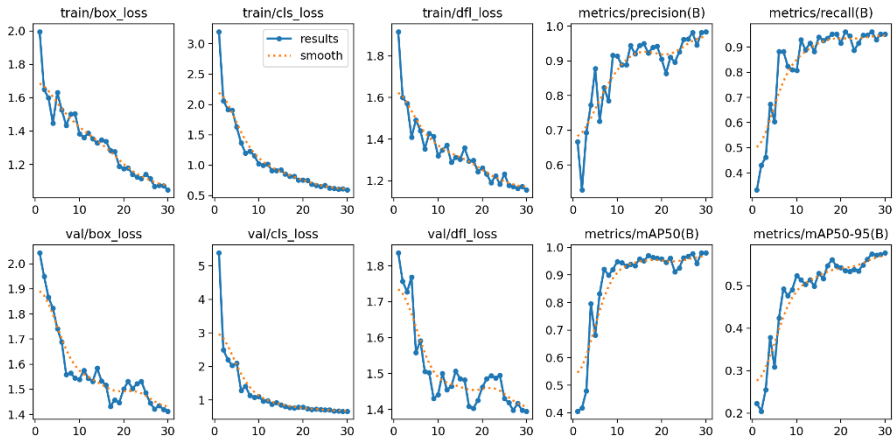

Figure 50: YOLOv8s 45° anatomical landmark detector training and validation metrics

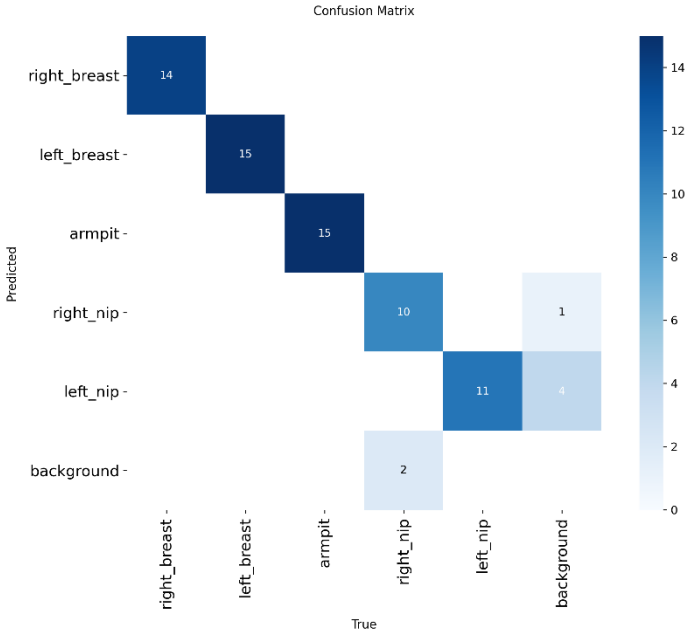

Figure 51: YOLOv8s 45° anatomical landmark detector confusion matrix

5.1.3 90° Models

5.1.3.1 Binary pose classifier

The YOLOv8cls model was trained for ?? epochs. The training and validation metrics are presented in Figure 52. The dataset used for training consisted of 195 binary 90° pose images, including 124 valid and 79 invalid samples. This dataset was split into 70% training (136 images), 15% validation (27 images), and 15% testing (32 images). The model achieved an inference time of 62.5 ms per image.

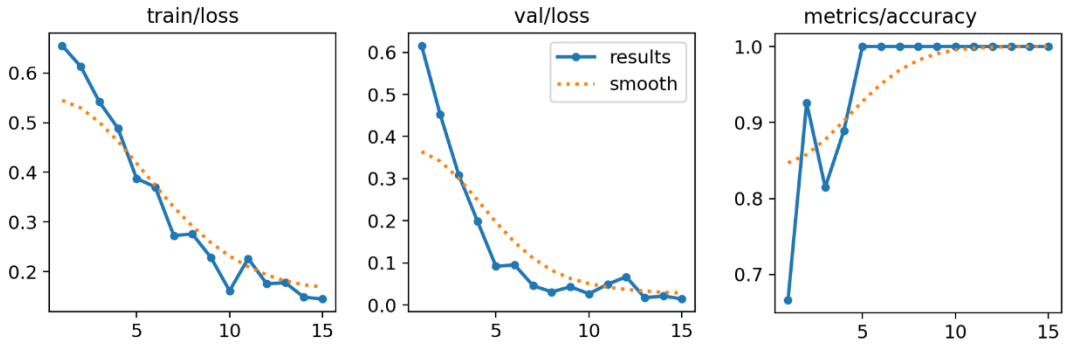

Figure 52: YOLOv8cls 90° binary pose classifier training and validation metrics

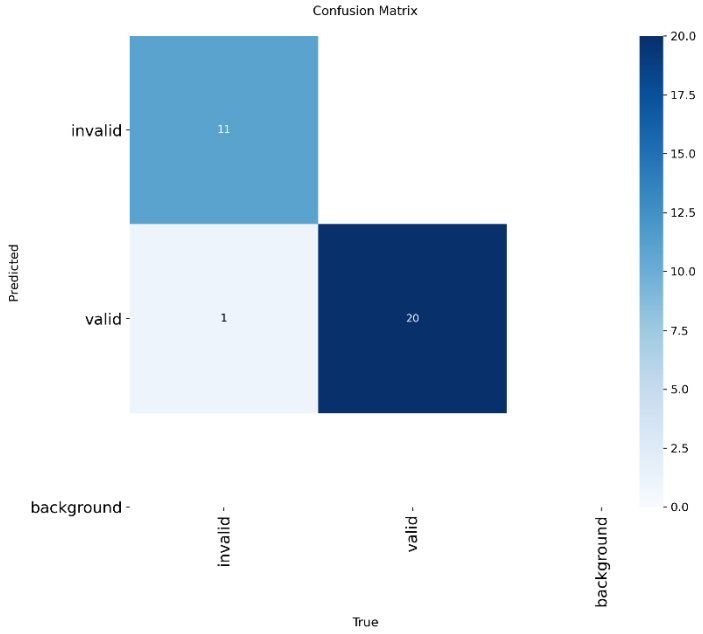

Figure 53: YOLOv8cls 90° binary pose classifier confusion matrix

5.1.3.2 Anatomical landmark detector

The YOLOv8s detector used for 90° anatomical landmark detection was trained for 25 epochs. The training and validation metrics are shown in Figure 54. The dataset consisted of 148 labeled images and was split into 80% training (118 images), 10% validation (14 images), and 10% testing (16 images). The model achieved an inference time of 122.1 ms per image.

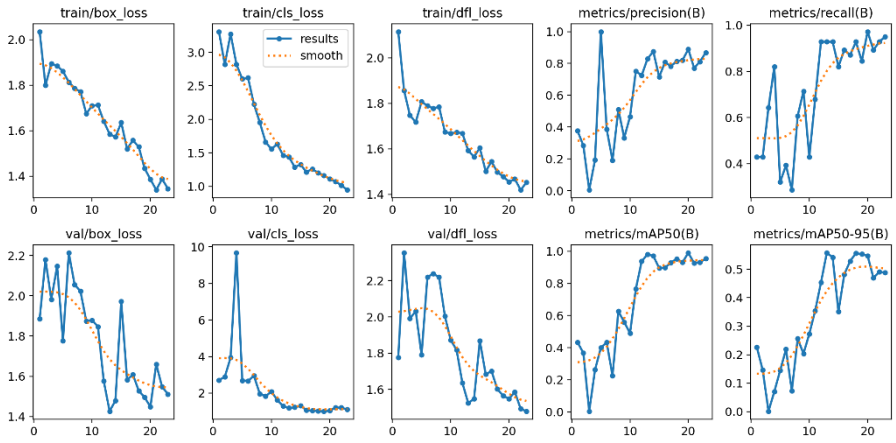

Figure 54: YOLOv8s 90° anatomical landmark detector training and validation results

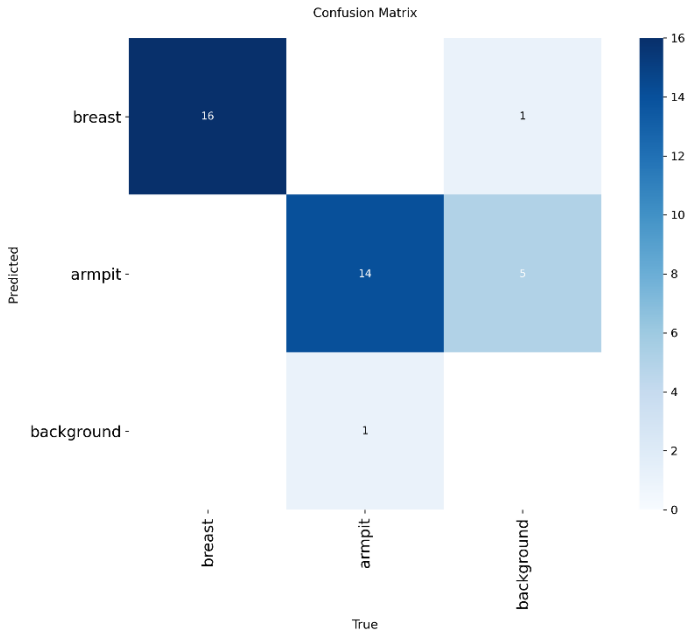

Figure 55: YOLOv8s 90° anatomical landmark detector confusion matrix

5.2 Sharpness Check Results

The sharpness check's purpose is to remove images that are clearly blurred. This is achieved by calculating the Laplacian variance of the image.

5.2.1 Thresholds

Frontal - 0° images: 10.0

45° images: 5.0

90° images: 7.0

5.2.2 Examples

From the examples shown in Figure 56 and Figure 57, it is evident that the algorithm, together with the selected thresholds, is able to distinguish between sharp and blurred images.

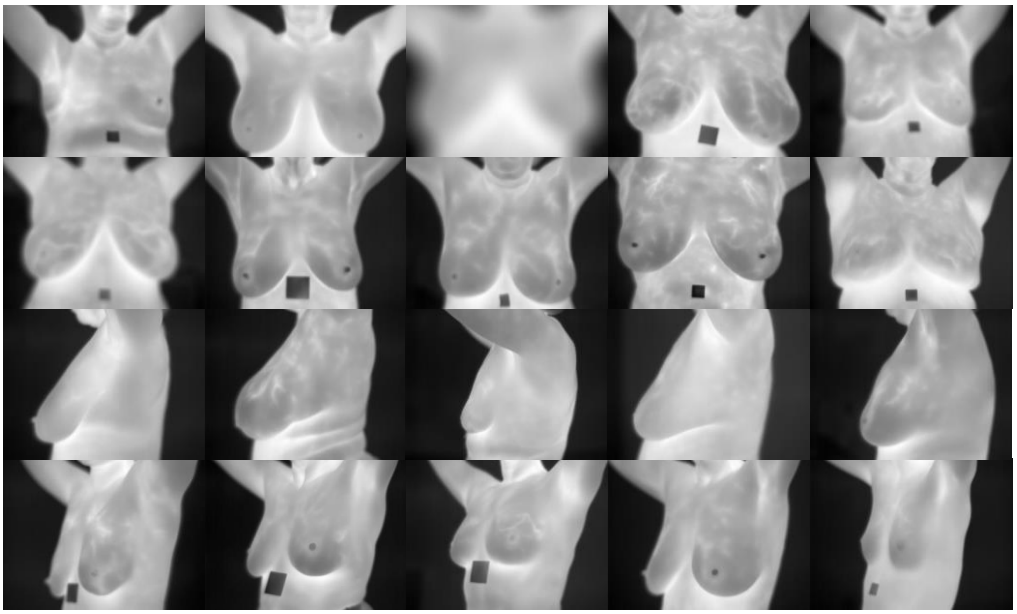

Figure 56: Multiple examples of images classified as blurry

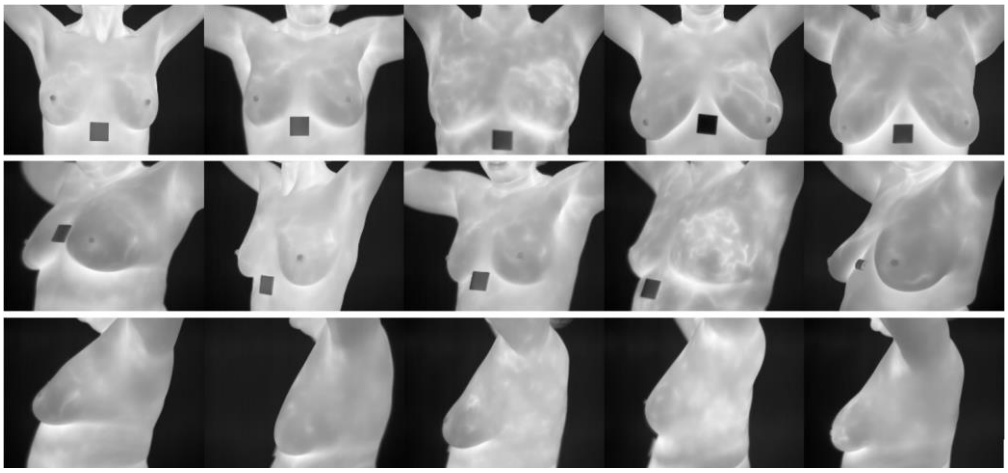

Figure 57: Examples of images classified as sharp

5.3 Binary Pose Check Results

The goal of the binary pose check is to reject binary masks that represent an incorrect or irregular patient pose. Details regarding the training, validation, and testing performance of the model used for this check are presented in the YOLO model metrics and results section.

5.3.1 Real examples

The model correctly classifies the only 4 images of incorrect poses shown in Figure 58 as invalid.

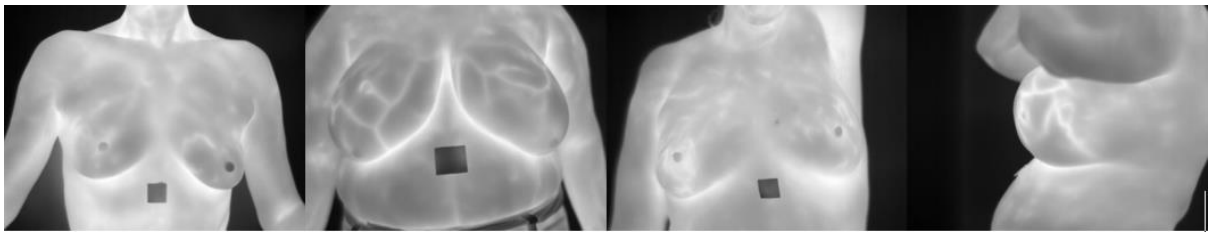

Figure 58: The only images with seriously incorrect poses in the dataset

5.4 Background Check Results

The goal of the background check is to verify that the image background is free of thermal activity and noise. This is achieved by computing the variance of the Laplacian response on the segmented background, as well as the mean intensity of background blocks, to identify unwanted thermal artefacts.

5.4.1 Thresholds

For all angles:

- Maximum Laplacian variance: 35.0
- Maximum mean intensity per 8 x 8 pixel block: 60.0

5.4.2 Examples:

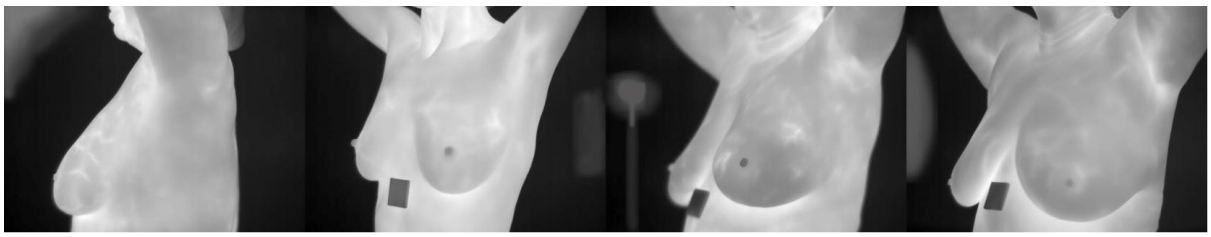

Figure 59: Images with faint thermal activity from objects in the background classified as invalid

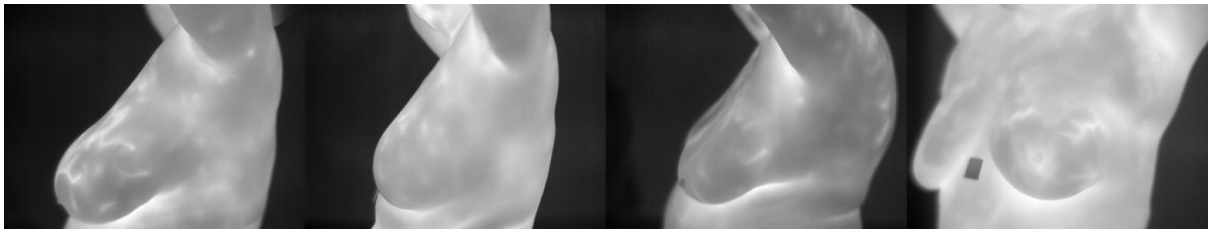

Figure 60: Images with mist-like thermal noise in the background classified as invalid

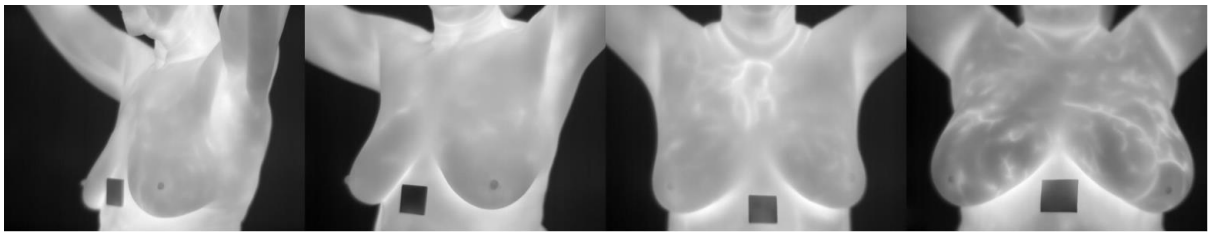

Figure 61: Images with minimal to no noise in the background classified as valid

5.5 Anatomical Landmark Analysis Results

The anatomical landmark detection checks ensure that key body landmarks are correctly detected and positioned within the image. Positional and geometric constraints are applied to verify proper framing, orientation, and pose for each viewing angle. Images that violate these constraints are rejected from further processing.

5.5.1 Thresholds

Frontal - 0° images:

- Minimum breast confidence score: 0.8
- Minimum armpit confidence score: 0.4
- Minimum nipple confidence score: 0.5
- Minimum breasts distance to image width ratio: 0.5
- Maximum breasts distance to image width ratio: 0.8
- Minimum breasts distance to armpits distance ratio: 1.0
- Maximum breasts distance to armpits distance ratio: 1.5
- Maximum absolute nipple angle: 12°
- Maximum absolute armpit angle: 15°
- Minimum distance to image borders: 0.08

- Maximum nipples and armpits midpoint horizontal distance: 0.2
- Maximum breasts midpoint offset to image midpoint: 0.2

45° images:

- Minimum right breast confidence score: 0.7
- Minimum armpit confidence score: 0.7
- Minimum left breast confidence score: 0.5
- Minimum nipple confidence score: 0.5
- Minimum distance to image borders: 0.05
- Maximum nipple horizontal distance to image width ratio: 0.45
- Minimum nipple horizontal distance to image width ratio: 0.25
- Maximum nipple angle: 20°
- Minimum nipple angle: -10°

90° images:

- Minimum breast confidence score: 0.7
- Minimum armpit confidence score: 0.5
- Minimum distance to image borders: 0.05
- Armpit center minimum horizontal position (normalized): 0.5
- Armpit center maximum horizontal position (normalized): 0.9
- Armpit center minimum height (normalized): 0.55
- Armpit center maximum height (normalized): 0.90
- Breast center minimum horizontal position (normalized): 0.25
- Breast center maximum horizontal position (normalized): 0.25
- Breast center minimum height position (normalized): 0.2
- Breast center maximum height position (normalized): 0.65

5.5.2 Examples

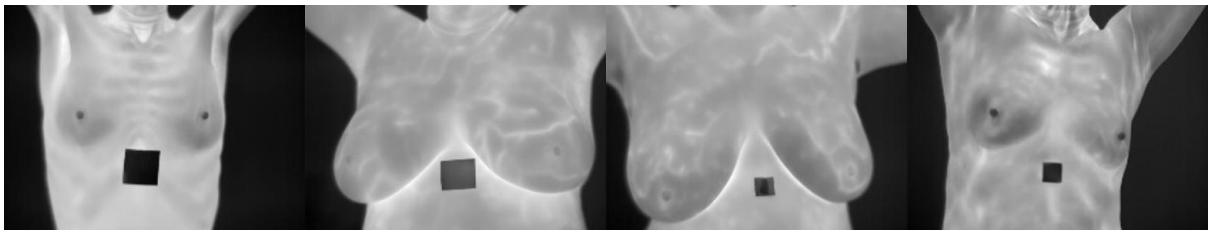

Figure 62: Frontal images with serious misalignments, classified as invalid

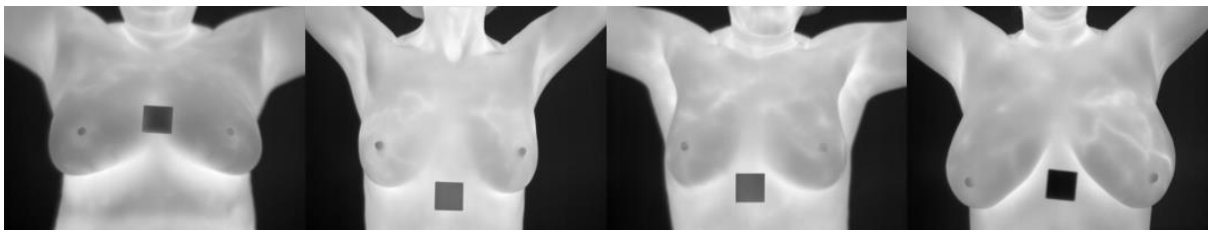

Figure 63: Frontal images properly aligned, classified as valid

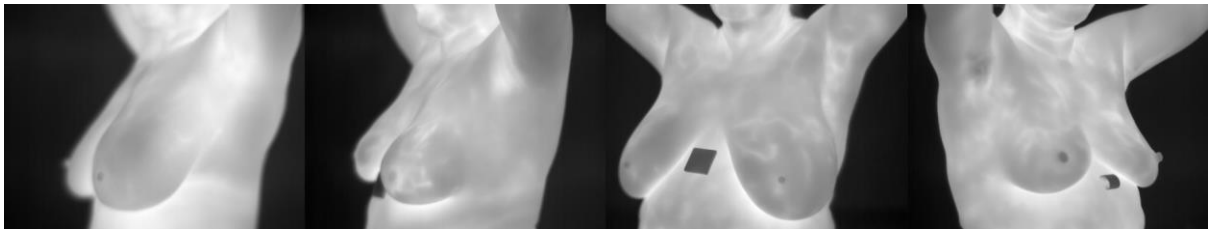

Figure 64: 45° images with serious misalignments, classified as invalid

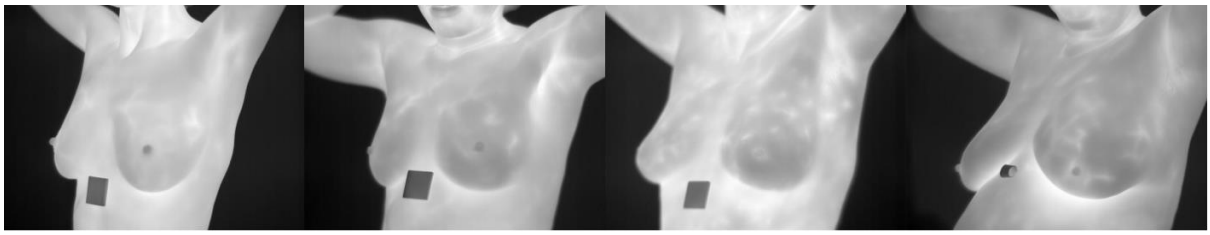

Figure 65: 45° images properly aligned, classified as valid

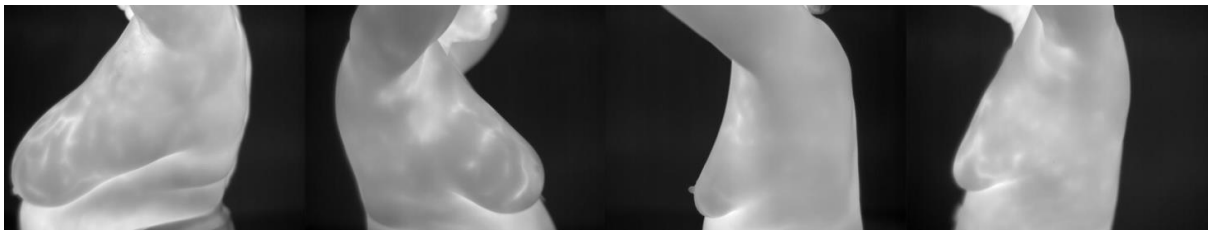

Figure 66: 90° images with misalignments and uncentered breasts, classified as invalid

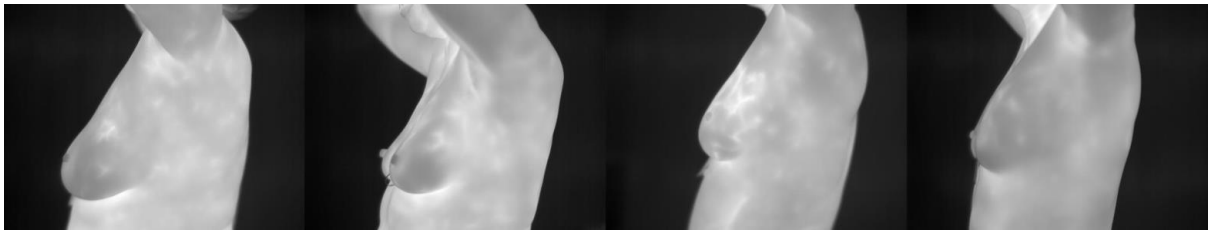

Figure 67: 90° images properly aligned and centered, classified as valid

5.6 Breast Band Quality Check Results

The breast band quality check assesses whether the chest region contains reliable and unobstructed thermal information. A combination of intensity-based and symmetry metrics is used to identify issues such as insufficient cooling, occlusions, or suppressed thermal patterns. Images that do not satisfy these criteria are classified as invalid and removed from further processing.

5.6.1 Thresholds

Frontal - 0° images:

- Breast mask top horizontal crop fraction: 0.20 (20% of the images top is cropped)
- Breast mask bottom horizontal crop fraction: 0.20
- Max symmetry ratio: 1.4
- Minimum mean intensity: 150.0
- Maximum mean intensity: 195.0
- Cold pixel threshold (κ): 0.8
- Maximum cold cluster area: 0.10
- Minimum intensity variance: 200.0

45° images:

- Breast mask top horizontal crop fraction: 0.30 (30% of the images top is cropped)
- Breast mask bottom horizontal crop fraction: 0.10
- Minimum mean intensity: 150.0
- Maximum mean intensity: 195.0
- Cold pixel threshold (κ): 0.8
- Maximum cold cluster area: 0.15
- Minimum intensity variance: 200.0

90° images:

- Breast mask top horizontal crop fraction: 0.30 (30% of the images top is cropped)
- Breast mask bottom horizontal crop fraction: 0.10
- Minimum mean intensity: 150.0
- Maximum mean intensity: 195.0
- Cold pixel threshold (κ): 0.9
- Maximum cold cluster area: 0.30
- Minimum intensity variance: 150.0

5.6.2 Examples

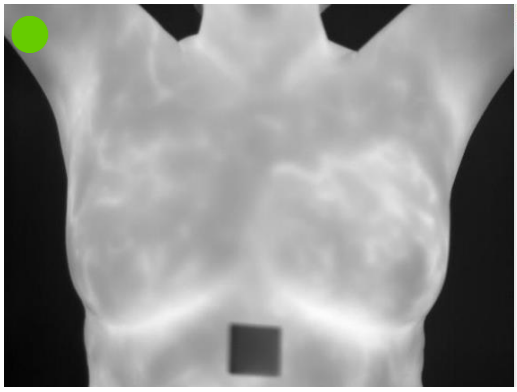

```
Breast metrics: {
 'coverage': 0.7074869791666667,
 'frac_top_border': 0.004110303364927456,
 'frac_bottom_border': 0.0027606515137572466,
 'cutoff_top_bottom': False,
 'area_left': 64288,
 'area_right': 66116,
 'symmetry_ratio': 1.028434544549527,
 'mean_intensity': 183.62948608398438,
 'var_intensity': 272.3626708984375,
 'min_intensity': 149.0,
 'max_intensity': 250.0,
 'dynamic_range': 101.0,
 'pct_low': 0.0,
 'pct_high': 9.969019355234503e-05,
 'cold_frac': 0.09420723290696605,
 'occlusion': False,
 'rules': {
  'no_cutoff': True,
  'symmetry_ok': True,
  'no_occlusion': True,
  'min_mean_ok': True,
  'max_mean_ok': True,
  'var_ok': True,
  'sat_low_ok': True,
  'sat_high_ok': True},
 'quality_ok': True}
```

Figure 68: Unedited frontal image that is classified as valid

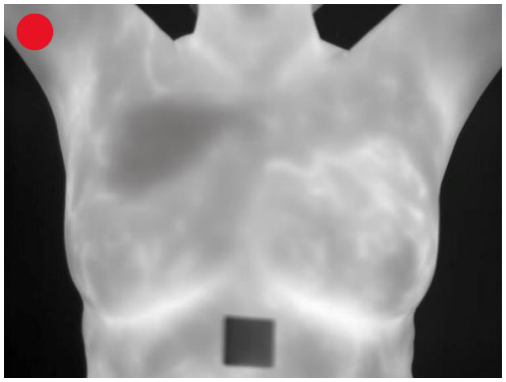

```
Breast metrics: {
 'coverage': 0.7076009114583334,
 'frac_top_border': 0.004109641556450067,
 'frac_bottom_border': 0.002783208740655549,
 'cutoff_top_bottom': False,
 'area_left': 64302,
 'area_right': 66123,
 'symmetry_ratio': 1.0283194923952599,
 'mean_intensity': 177.7887420654297,
 'var_intensity': 551.5618896484375,
 'min_intensity': 114.0,
 'max_intensity': 250.0,
 'dynamic_range': 136.0,
 'pct_low': 0.0,
 'pct_high': 9.967414222733372e-05,
 'cold_frac': 0.12907034694268738,
 'occlusion': True,
 'rules': {
  'no_cutoff': True,
  'symmetry_ok': True,
  'no_occlusion': False,
  'min_mean_ok': True,
  'max_mean_ok': True,
  'var_ok': True,
  'sat_low_ok': True,
  'sat_high_ok': True},
 'quality_ok': False,
 'reason': 'rules_failed'}
```

Figure 69: Edited frontal image that includes a cold spot above the left breast, the image is classified as invalid due to an occlusion

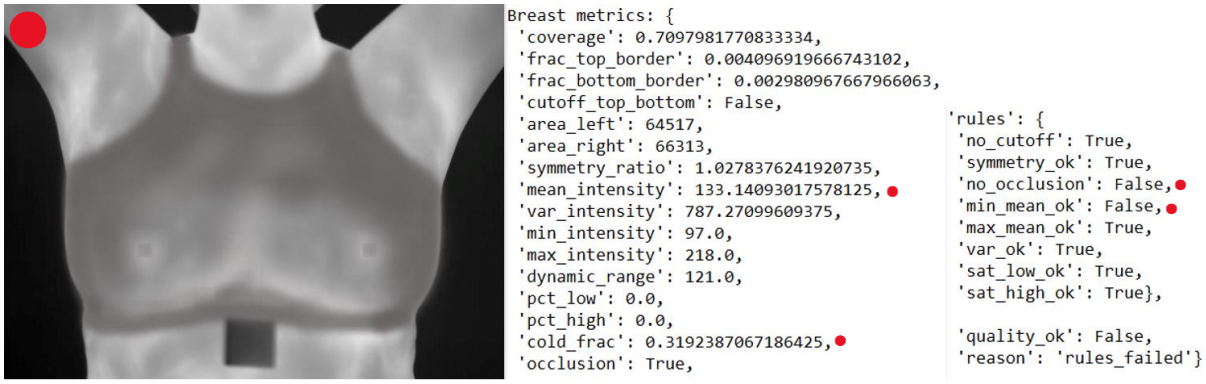

Figure 70: Edited frontal image that shows a patient wearing clothing, classified as invalid due to an occlusion and low intensity mean

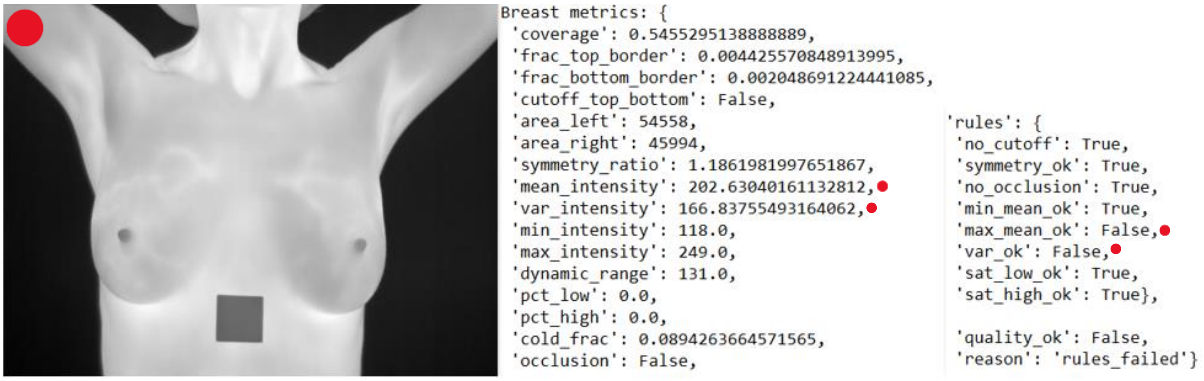

Figure 71: Unedited frontal image showing a patient with high body temperature with blood vessels not highlighted properly, classified as invalid due to high intensity mean and low intensity variance

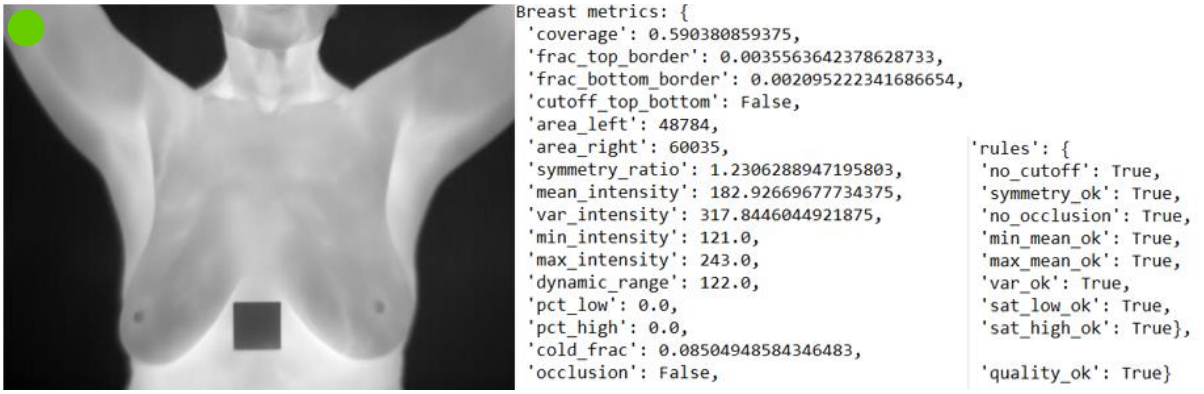

Figure 72: Unedited frontal image of a patient, classified as valid

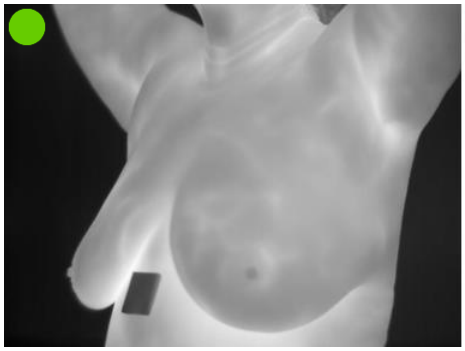

```
Breast metrics: {
 'coverage': 0.7052588383838384,
 'frac_top_border': 0.004243015584578339,
 'frac_bottom_border': 0.003034561778844002,
 'cutoff_top_bottom': False,
 'mean_intensity': 166.8066864013672,
 'var_intensity': 255.30894470214844,
 'min_intensity': 111.0,
 'max_intensity': 249.0,
 'dynamic_range': 138.0,
 'pct_low': 0.0,
 'pct_high': 0.0,
 'cold_frac': 0.08075156875207004,
 'occlusion': False,
 'rules': {
  'no_cutoff': True,
  'no_occlusion': True,
  'min_mean_ok': True,
  'max_mean_ok': True,
  'var_ok': True,
  'sat_low_ok': True,
  'sat_high_ok': True},

  'quality_ok': True}
```

Figure 73: Unedited 45° image, classified as valid

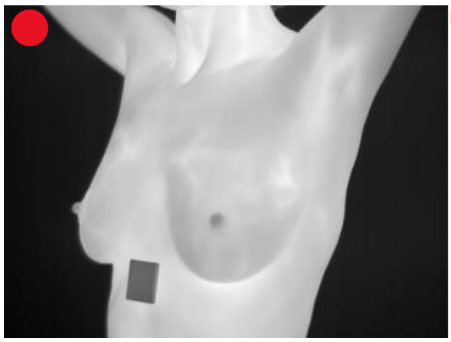

```
Breast metrics: {
 'coverage': 0.6376044489611563,
 'frac_top_border': 0.003741172824474797,
 'frac_bottom_border': 0.002235848847763044,
 'cutoff_top_bottom': False,
 'mean_intensity': 202.00048828125,
 'var_intensity': 124.44207000732422,
 'min_intensity': 141.0,
 'max_intensity': 245.0,
 'dynamic_range': 104.0,
 'pct_low': 0.0,
 'pct_high': 0.0,
 'cold_frac': 0.12377969140858477,
 'occlusion': False,
 'rules': {
  'no_cutoff': True,
  'no_occlusion': True,
  'min_mean_ok': True,
  'max_mean_ok': False,
  'var_ok': False,
  'sat_low_ok': True,
  'sat_high_ok': True},

  'quality_ok': False,
  'reason': 'rules_failed'}
```

Figure 74: Unedited 45° image showing a patient with high body temperature and blood vessels not properly highlighted, classified as invalid due to high intensity mean and low intensity variance

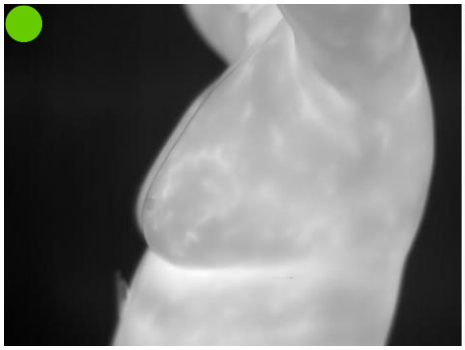

```
Breast metrics: {
 'coverage': 0.7921820086509868,
 'frac_top_border': 0.002548816773133978,
 'frac_bottom_border': 0.003561944779191417,
 'cutoff_top_bottom': False,
 'mean_intensity': 188.88099670410156,
 'var_intensity': 188.3887176513672,
 'min_intensity': 155.0,
 'max_intensity': 253.0,
 'dynamic_range': 98.0,
 'pct_low': 0.0,
 'pct_high': 0.001375721187172733,
 'cold_frac': 0.048352867152257145,
 'occlusion': False,
 'rules': {
  'no_cutoff': True,
  'no_occlusion': True,
  'min_mean_ok': True,
  'max_mean_ok': True,
  'var_ok': True,
  'sat_low_ok': True,
  'sat_high_ok': True},

  'quality_ok': True}
```

Figure 75: Unedited 90° image, classified as valid

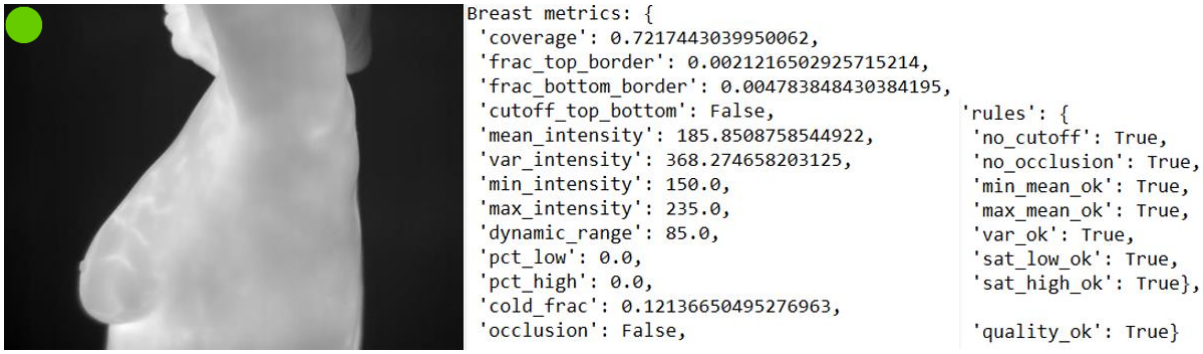

Figure 76: Unedited 90° image, classified as valid

5.7 Pipeline Overall Performance

Since the pipeline is designed as a strictly sequential process, failure at any individual check results in the image being rejected from further processing. The examples presented in the previous subsections demonstrate that each check successfully identifies the type of quality issue it was designed to detect. As a result, images that violate acquisition protocols are consistently filtered out before reaching later stages, while images that satisfy all requirements proceed through the pipeline. This behavior confirms that the pipeline operates as intended and enforces the quality constraints defined in this work.

6 Discussion

6.1 Experimental Setup

All experiments were conducted on an HP Pavilion 15 laptop equipped with an AMD Ryzen 7 processor, integrated AMD Radeon graphics, and 16 GB of system memory. The host operating system was Windows, while all development and experimental execution took place within an Ubuntu Linux virtual machine. Due to the absence of a dedicated GPU, all model training and inference were performed on the CPU.

The pipeline and all supporting experiments were implemented in Python using Visual Studio Code running inside the Ubuntu virtual machine. Image processing operations were carried out using OpenCV and NumPy, while the deep learning components were implemented using the Ultralytics YOLOv8 framework built on PyTorch. Despite the lack of GPU acceleration, the experimental setup was sufficient to evaluate the behavior and performance of the proposed quality assessment pipeline, as the focus of this work lies on rule-based validation and lightweight model inference rather than large-scale model training.

6.2 Interpretation of Results

The results presented in the previous sections demonstrate that the proposed pipeline behaves as intended and enforces the quality constraints defined in this work. Since the pipeline operates sequentially, images that fail any individual check are immediately rejected, preventing low-quality inputs from reaching later stages. The examples provided show that each check consistently identifies the specific type of screening issue it was designed to detect.

The sharpness and background quality checks effectively remove images affected by blur or unwanted thermal activity in the background, ensuring that subsequent analysis is performed only on clear and stable inputs. The binary pose and anatomical landmark checks further verify that the patient is correctly positioned and oriented for each viewing angle, rejecting images with incorrect posture, framing, or landmark geometry. Finally, the breast band quality check identifies cases where thermal information is unreliable due to insufficient cooling or occlusions, addressing issues that are not easily detected through pose or background analysis alone.

Overall, the results indicate that the proposed pipeline establishes a solid foundation for automated quality assessment in thermal breast cancer screening. By systematically filtering images that violate acquisition and quality constraints, the pipeline defines a structured approach for ensuring reliable input data prior to breast cancer classification. This work therefore sets the groundwork for future automated screening systems that depend on consistent and high-quality thermal imagery.

6.3 Limitations

While the proposed pipeline demonstrates consistent and meaningful behavior, several limitations should be acknowledged. First, the evaluation was conducted using the DMR-IR dataset, which was collected under controlled conditions and contains relatively few images with severe acquisition errors. As a result, some failure cases, particularly those related to arm positioning, occlusions and insufficient cooling, were manually introduced in order to evaluate the robustness of the proposed checks. Although this approach allows controlled testing of specific failure modes, it does not fully capture the variability expected in real-world screening scenarios and forces the pipeline to rely on older image processing techniques due to the inability of using neural networks.

Another limitation lies in the rule-based nature of several pipeline components. Threshold values for the different quality metrics were selected empirically and heuristically based on a visual inspection and iterative testing. While these thresholds were effective for the dataset and scenarios examined in this work, they may require adjustment when applied to different thermal cameras, acquisition environments, or patient populations.

Finally, the pipeline focuses exclusively on image quality assessment and does not attempt to perform diagnostic interpretation. While this separation is intentional, it means that the direct impact of the proposed pipeline on breast cancer classification accuracy was not quantitatively evaluated within this thesis.

These limitations highlight opportunities for future work, particularly in evaluating the pipeline on larger and more diverse datasets and integrating adaptive thresholding strategies.

7 Conclusion & Future Work

7.1 Conclusion

This thesis presented a rule-based quality assessment pipeline designed to evaluate thermal breast images prior to automated breast cancer classification. The proposed pipeline addresses common acquisition issues by systematically verifying image sharpness, background cleanliness, patient pose, anatomical landmark geometry, and breast band thermal quality. By enforcing these checks sequentially, the pipeline ensures that only images meeting predefined quality criteria are passed to downstream analysis.

The results demonstrate that each individual check behaves as intended and effectively identifies the specific type of quality issue it was designed to detect. Through qualitative examples and threshold-based evaluation, the pipeline was shown to reliably filter images affected by blur, incorrect positioning, background thermal artefacts, occlusions, or insufficient cooling. This structured approach helps standardize input conditions and reduces the risk of unreliable predictions caused by poor-quality thermal data.

The development of the proposed pipeline was informed by guidance from MammoCheck, a startup working toward automated breast cancer detection using thermal imaging. This guidance helped shape the practical requirements and constraints considered in this work, particularly with respect to acquisition consistency and image quality validation. Within this context, the pipeline establishes a foundation for automated quality assessment that supports reliable data preparation for downstream analysis.

Overall, this thesis contributes a practical and systematic approach to thermal image quality control that aligns with the needs of emerging automated screening systems, including those envisioned by MammoCheck. The methods and insights presented here provide a modular framework that can be extended and adapted to future thermal imaging workflows, supporting the development of more robust and trustworthy breast cancer screening solutions.

7.2 Future Work

Several directions can be explored to extend and improve the work presented in this thesis. A natural next step is the evaluation of the proposed pipeline on larger and more diverse datasets, including images collected in less controlled environments such as clinical screenings conducted by non-expert operators or home-based self-screening scenarios. In addition, future datasets could include a greater number of images exhibiting incorrect poses, positioning errors, and framing issues, allowing for more extensive testing and refinement of the pose and landmark validation checks. This would enable a more comprehensive assessment of the pipeline's robustness under real-world conditions.

Future work could also focus on reducing the reliance on manually selected threshold values. Adaptive or data-driven thresholding strategies could be investigated, allowing the quality checks to adjust automatically to different thermal cameras, acquisition setups, or patient populations. Incorporating statistical modeling or lightweight learning-based components may further improve the generalization of the pipeline or allow it to be dynamically adapted to datasets that follow different capture protocols.

Another promising direction is the tighter integration of the quality assessment pipeline with downstream breast cancer classification models. Evaluating the impact of quality filtering on diagnostic performance would provide quantitative insight into how input quality affects classification reliability. In addition, real-time feedback mechanisms could be developed to guide patients or operators during image acquisition, helping them correct issues such as pose, distance, or occlusions before the image is captured.

Finally, future implementations could explore optimizing the computational performance of the pipeline to support real-time or near real-time operation on resource-constrained devices. This would be particularly important for deployment in portable screening systems or mobile applications, where efficiency and responsiveness are critical.

8 References

[1] E. F. J. A. K. Ring, "Infrared thermal imaging in medicine," *Physiological Measurement,* vol. 33, no. 3, pp. R33-R46, 2012.

[2] J. C. Fernandes, A. F. Mifuel and P. Matias, "Influence of acquisition conditions on thermal imaging," *Infrared Physics & Technology,* vol. 73, pp. 123-134, 2015.

[3] M. Pafitis, "An affordable and safe method for breast cancer examinations at home," Nicosia, 2023.

[4] G. W. H. I. S. D. Shen, "Deep learning in medical image analysis," *Annual Review of Biomedical Engineering,* vol. 19, pp. 221-248, 2017.

[5] M. L. D. B. S. E. B. M. T. K. S. K. Brian M. Sanchez, "Use of a portable thermal imaging unit as a rapid, quantitative method of evaluating inflammation and experimental arthritis," *Journal of Pharmacological and Toxicological Methods,* vol. 57, no. 3, pp. 169-175, 2008.

[6] S. Bagavathiappan, T. Saravanan, J. Philip, T. Jayakumar, B. Raj, R. Karunanithi, T. M. R. Panicker, M. P. Korath and K. Jagadeesan, "Infrared thermal imaging for detection of peripheral vascular disorders," *Journal of Medical Physics,* vol. 34, no. 1, pp. 43-47, 2009.

[7] P. F. V. O. D. C. R. &. G. N. M. Sousa, "A review of thermal methods and technologies for diabetic foot assessment," *Expert Review of Medical Devices,* vol. 12, no. 4, pp. 439-448, 2015.

[8] G. M. H. M. a. H. V. R. S. T. Kakileti, "Advances in Breast Thermography," in *New Perspectives in Breast Imaging*, InTech, 2017, pp. 91-108.

[9] E. M. S. Elad, "Image quality assessment for medical imaging: A review," *Information Fusion,* vol. 45, pp. 1-20, 2019.

[10] Z. Zheng, Y. Huang and L. Guo, "Deep Learning-Based Human Pose Estimation: A Survey," *IEEE Transactions on Pattern Analysis and Machine Intelligence,* vol. 44, no. 6, pp. 3239-3255, 2022.

[11] Z. Cao, T. Simon, S.-E. Wei and Y. Sheikh, "OpenPose: Realtime Multi-Person 2D Pose Estimation using Part Affinity Fields," *IEEE Transactions on Pattern Analysis and Machine Intelligence,* vol. 43, no. 1, pp. 172-186, 2021.

[12] X. Fang, R. Yang and X. Li, "Human pose estimation from monocular images: A comprehensive survey," *Sensors,* vol. 22, no. 21, 2022.

[13] D. W. a. L. Shao, "Silhouette Analysis-Based Action Recognition Via Exploiting Human Poses," *Transactions on Circuits and Systems for Video Technology,* vol. 23, no. 2, pp. 236-243, 2013.

[14] G. Jocher, A. Chaurasia and J. Qiu, "YOLOv5," Ultralytics, 2020.

[15] C. Dong and G. Du, "An enhanced real-time human pose estimation method based on modified YOLOv8 framework," *Scientific Reports,* vol. 14, no. 8012, 2024.

[16] J. Yang, Z. Li, Y. Zhang, X. Zhou and Y. Xu, "Deep learning-based anatomical landmark detection in medical images: a review," *Computers in Biology and Medicine,* vol. 141, 2022.

[17] Y. Guan and C. He, "Segmentation of Thermal Breast Images Using Convolutional Neural Networks," in *2018 47th Applied Imagery Pattern Recognition Workshop (AIPR)*, 2018.

[18] L. Lou, S. Li and J. Liu, "Segmentation of Infrared Breast Images Using Graph-Based Approaches," *Infrared Physics & Technology,* 2020.

[19] A. Mohamed, R. Abdalla and e. al., "Deep Learning Model for Fully Automated Breast Cancer Detection from Thermograms," *Applied Sciences,* vol. 12, 2022.

[20] E. Y. K. Ng, "A review of thermography as promising non-invasive detection modality for breast tumor," *International Journal of Thermal Sciences,* vol. 48, pp. 849-859, 2009.

[21] N. Arora, "Effectiveness of a Noninvasive Digital Infrared Thermal Imaging System in the Detection of Breast Cancer," *The American Journal of Surgery,* vol. 196, no. 4, pp. 523-526, 2008.

[22] D. C. M. S. G. O. S. O. A. S. A. P. R. B. A. C. L. F. Silva, "A New Database for Breast Research with Infrared Image," *Journal of Medical Imaging and Health Informatics,* vol. 3, no. 1, pp. 92-100, 2014.

[23] A. Lemay, "Kidney Recognition in CT Using YOLOv3,," Montreal, 2019.

Appendix

The source code including the pipelines and the YOLOv8 models training datasets can be found in the github repository shown below.

https://github.com/A-Tamanis/Thermal-Image-Quality-Assessment-and-Validation-for-Breast-Cancer-Classifier-Inference